ARTICLE

Nesprins are mechanotransducers that discriminate epithelial–mesenchymal transition programs

Théophile Déjardin[1]*, Pietro Salvatore Carollo[1]*, François Sipieter[1], Patricia M. Davidson[2], Cynthia Seiler[1], Damien Cuvelier[3], Bruno Cadot[4], Cecile Sykes[2], Edgar R. Gomes[4,5,6], and Nicolas Borghi[1]

LINC complexes are transmembrane protein assemblies that physically connect the nucleoskeleton and cytoskeleton through the nuclear envelope. Dysfunctions of LINC complexes are associated with pathologies such as cancer and muscular disorders. The mechanical roles of LINC complexes are poorly understood. To address this, we used genetically encoded FRET biosensors of molecular tension in a nesprin protein of the LINC complex of fibroblastic and epithelial cells in culture. We exposed cells to mechanical, genetic, and pharmacological perturbations, mimicking a range of physiological and pathological situations. We show that nesprin experiences tension generated by the cytoskeleton and acts as a mechanical sensor of cell packing. Moreover, nesprin discriminates between inductions of partial and complete epithelial–mesenchymal transitions. We identify the implicated mechanisms, which involve α-catenin capture at the nuclear envelope by nesprin upon its relaxation, thereby regulating β-catenin transcription. Our data thus implicate LINC complex proteins as mechanotransducers that fine-tune β-catenin signaling in a manner dependent on the epithelial–mesenchymal transition program.

Introduction

The cell nucleus is not only the repository of the genome but also the largest organelle in most cells, whose shape response to mechanical cues was shown close to a century ago (Chambers and Fell, 1931). The cytoskeleton mechanically couples the nucleus to cell adhesion complexes such that extracellular mechanical cues can affect the position and shape of the nucleus (Maniotis et al., 1997). Such mechanical coupling is provided by outer nuclear transmembrane proteins, called "nesprins," whose KASH domain interacts with inner nuclear transmembrane SUN proteins in the perinuclear space (Lombardi et al., 2011). The cytoplasmic domain of nesprins can bind to the cytoskeleton and the nucleoplasmic domain of SUNs can bind to the nucleoskeleton to form the so-called LINC complex: linker of nucleoskeleton and cytoskeleton (Crisp et al., 2006).

Mutations in or loss of LINC complex proteins impair a variety of functions, including nuclear envelope integrity (Crisp et al., 2006), nucleus anchoring (Starr and Han 2002; Grady et al., 2005), signaling to the nucleus (Neumann et al., 2010), chromosome positioning (Chikashige et al., 2006), DNA repair (Swartz et al., 2014), genome transcription (Alam et al., 2016),

and replication (Wang et al., 2018), which impact cell polarity, migration, division, or differentiation in a variety of contexts. More recently, disruption of the LINC complex was shown to impair the induction by extracellular mechanical cues of chromatin stretching and transcription (Tajik et al., 2016) and nuclear translocation of transcription cofactors (Driscoll et al., 2015; Elosegui-Artola et al., 2017; Uzer et al., 2018). Genetically encoded biosensors of tension in nesprins now exist (Arsenovic et al., 2016), and direct force application on nesprins was shown to elicit nucleus-autonomous signaling that targets nucleus stiffness (Guilluy et al., 2014). Yet it is still unclear whether the consequences of LINC complex disruption as described above result from an impairment of mechanotransduction within the LINC complex itself. Alternatively, they could result from a mere loss of mechanostructural integrity or even of a nonmechanical function. Thus, the mechanistic determinants of LINC complex cellular functions and their involvement in the many associated diseases mostly remain to be discovered (Janin et al., 2017).

Here, we focused on nesprin-2 giant (nesprin-2G), a nesprin involved in nucleus positioning during cell polarization in

[1]Université de Paris, Centre National de la Recherche Scientifique, Institut Jacques Monod, Paris, France; [2]Laboratoire Physico-Chimie Curie, Institut Curie, Centre National de la Recherche Scientifique Unité Mixte de Recherche 168, Sorbonne Universités, Université Paris Sciences et Lettres, Paris, France; [3]Institut Curie and Institut Pierre Gilles de Gennes, Université Paris Sciences et Lettres, Centre National de la Recherche Scientifique Unité Mixte de Rercherche 144, Paris, France; [4]Center for Research in Myology, Institut National de la Santé et de la Recherche Médicale Unité Mixte de Recherche 974, Sorbonne Universités, Paris, France; [5]Instituto de Medecina Molecular, Faculdade de Medicina, Universidade de Lisboa, Lisboa, Portugal; [6]Instituto de Histologia e Biologia do Desenvolvimento, Faculdade de Medicina, Universidade de Lisboa, Lisboa, Portugal.

*T. Déjardin and P.S. Carollo contributed equally to this paper;   Correspondence to Nicolas Borghi: nicolas.borghi@ijm.fr.

migrating fibroblasts (Luxton et al., 2010; Borrego-Pinto et al., 2012). Nesprin-2G forms a complex with and regulates the nuclear localization of β-catenin (Neumann et al., 2010), a major transcription cofactor in several morphogenetic processes. We had previously shown that, upon induction of partial or complete epithelial–mesenchymal transition (EMT; Jolly et al., 2017; Aiello et al., 2018), epithelial cell packing regulates β-catenin signaling (Gayrard et al., 2018). We hypothesized that nesprins could participate in this mechanical regulation.

We combined molecular tension microscopy (Gayrard and Borghi, 2016) with mechanical, genetic, and pharmacological perturbations of fibroblastic and epithelial cells in culture. We found that nesprin is mechanosensitive to cell packing. Moreover, nesprin tension increases upon induction of partial but not complete EMT, thereby defining two mechanisms of β-catenin nuclear translocation. Upon induction of complete EMT, nesprin relaxation causes α-catenin recruitment at the nuclear envelope, which results in nuclear translocation of both catenins. Upon partial EMT, however, tensed nesprin does not recruit α-catenin, and only β-catenin translocates to the nucleus. Finally, we found that α-catenin sequesters β-catenin in the nucleus in a transcriptionally less active form.

Results

Nesprin is under cytoskeleton-dependent tension balanced by cell adhesion

To assess the tension exerted on nesprin, we generated a short variant of nesprin-2G known to rescue the nucleus-positioning function of the full-length protein (Luxton et al., 2010) with a tension sensor module (TSMod; Grashoff et al., 2010) consisting of a pair of fluorescent proteins flanking a polypeptidic spring (Fig. 1 A). The tension sensor is inserted between the transmembrane domain and the neighboring spectrin repeat (SR). When transiently expressed in Madin-Darby canine kidney (MDCK) cells, this construct exhibited a Förster resonance energy transfer (FRET) index that did not depend on its level of expression over greater than an order of magnitude in expression level (Fig. S1 A). This excludes any substantial contribution to FRET changes of intermolecular FRET or of force imbalance subsequent to endogenous nesprin displacement. Consistently, we found that NIH 3T3 cells expressing the construct retained nesprin-1G at the nuclear envelope (Fig. S1 B). For tension-insensitive controls, we designed a short variant bearing mutations in the calponin homology (CH) domain that impair interaction with the cytoskeleton (CH mutant; Luxton et al., 2010), a truncated variant lacking its cytoplasmic part (dominant-negative KASH [DNKASH]), and a short variant with the TSMod appended beyond the CH domain (Beyond; Fig. 1 A). As expected, colonies of MDCK and NIH 3T3 cells stably expressing the construct able to bind the cytoskeleton (CB) exhibited a FRET index significantly lower than that of the CH mutant, supporting that the CB construct is under mechanical tension due to specific interaction with the cytoskeleton (Fig. 1, B and C). Surprisingly, the two other control constructs exhibited FRET indices lower than that of the CH mutant and in most cases indistinguishable from that of the CB construct (Fig. 1, B and C). The DNKASH and

Beyond constructs both differ from the CH mutant (and CB) in the local environment of the sensor, which is no longer flanked by a cytoplasmic domain on the side opposite the transmembrane domain. The lower FRET of DNKASH and Beyond constructs supports that the cytoplasmic domain acts as a steric hindrance that exerts a compression on the sensor in the CH mutant construct, as previously seen in the other SR protein α-actinin (Rahimzadeh et al., 2011). The same effect occurs in the CB and CH mutant constructs, in which the sensor shares the same environment, although the increase in FRET is alleviated upon specific interaction with the cytoskeleton in the CB construct. Therefore, the CH mutant construct is a truer FRET reference than DNKASH or Beyond for cytoskeleton-dependent tension. Finally, both CB and CH mutant constructs preserved nesprin-1G localization at the nuclear envelope (Fig. S1 B), further supporting their functional similarity, actin binding apart. We thus used the CB and CH mutant constructs to further assess cytoskeleton-dependent changes in tension.

In MDCK cells exposed to either the actin polymerization inhibitor cytochalasin D, the ROCK inhibitor Y27632, or the microtubule polymerization inhibitor colchicine, the CB construct exhibited a significant FRET index increase (Fig. 1, D and E). This supports that nesprin-2G tension requires dynamic microtubules and a contractile actomyosin network, which is perturbed in these conditions (Fig. S1 C). In contrast, the CH mutant did not exhibit significant FRET index changes in those conditions (Fig. S1 D and Fig. 1 E), indicating that disrupting actomyosin or microtubules does not further relieve tension when the cytoskeleton-binding domain is mutated. The tension generated by the cytoskeleton is thus exerted through the intact CH domain exclusively. Moreover, because these mutations do not completely impair cytoskeleton binding, the full loss of binding is not essential to lose force sensitivity.

We next examined how the cytoskeleton-generated tension exerted on nesprin-2G was balanced. To do so, we perturbed calcium-dependent cell adhesion in MDCK cells by exposure to the calcium chelator EDTA (Fig. S1 C). Impaired cell adhesion resulted in an increase of FRET index in the CB construct, but not in the CH mutant (Fig. 1, D and E; and Fig. S1 D). This supports that cell adhesion is involved to balance the cytoskeletal tension on nesprin-2G. We thus sought to assess nesprin sensitivity to extracellular mechanical cues.

Nesprin tension is sensitive to extracellular mechanical cues

To test nesprin sensitivity to extracellular mechanical cues, we first allowed MDCK and NIH 3T3 cells to individually migrate through an array of obstacles with constrictions smaller than the nucleus diameter (Davidson et al., 2015). As cells migrated through constrictions, nucleus squeezing was accompanied by an increase in FRET index of the CB construct in nuclear regions within constrictions compared with regions outside constrictions (Fig. 2, A and B). In contrast, the CH mutant exhibited an increase in FRET within constrictions that was not statistically significant (Fig. S2, A and B). Therefore, these results support that cell migration through narrow constrictions reduces cytoskeleton-generated tension on nesprin-2G in the region that is squeezed.
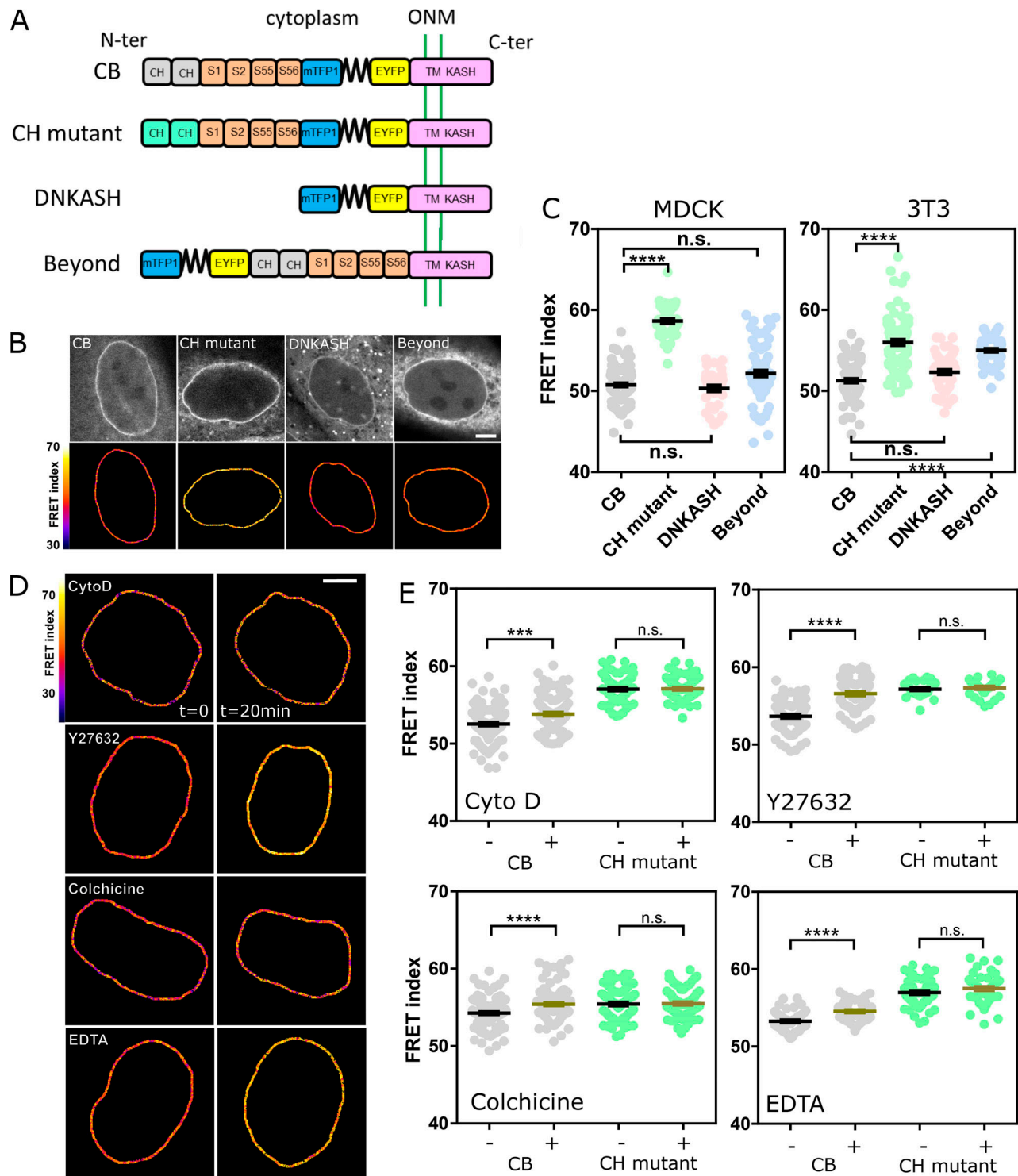
Figure 1. **Nesprin is under cytoskeleton-dependent tension. (A)** Schematics of the nesprin constructs. CB and CH^2 domains. ONM, outer nuclear membrane; S1...S56, spectrin repeat number; TM, transmembrane. **(B)** Typical nuclei expressing the nesprin constructs above. Top: Direct fluorescence. Bottom: FRET index map. **(C)** FRET index of the nesprin constructs above in MDCK (left; n = 97 CB, 45 CH mutant, 34 DNKASH, 35 Beyond) and NIH 3T3 (right; n = 88 CB, 89 CH mutant, 60 DNKASH, 62 Beyond) cells; three replicates. **(D)** FRET index map of the CB construct in MDCK cells before and after 20 min of pharmacological perturbation. Cyto D, cytochalasin D. **(E)** FRET index of the CB construct and the CH mutant in MDCK cells before and after pharmacological perturbation (n Cyto D = 108 CB, 71 CH mutant; n Y27632 = 74 CB, 30 CH mutant; n colchicine = 112 CB, 88 CH mutant; n EDTA = 48 CB, 52 CH mutant); two replicates. Scale bars = 5 µm. Mean ± SEM. Two-tailed Kruskal-Wallis (C) and Mann-Whitney (E) tests. ***, P < 0.001; ****, P < 0.0001.
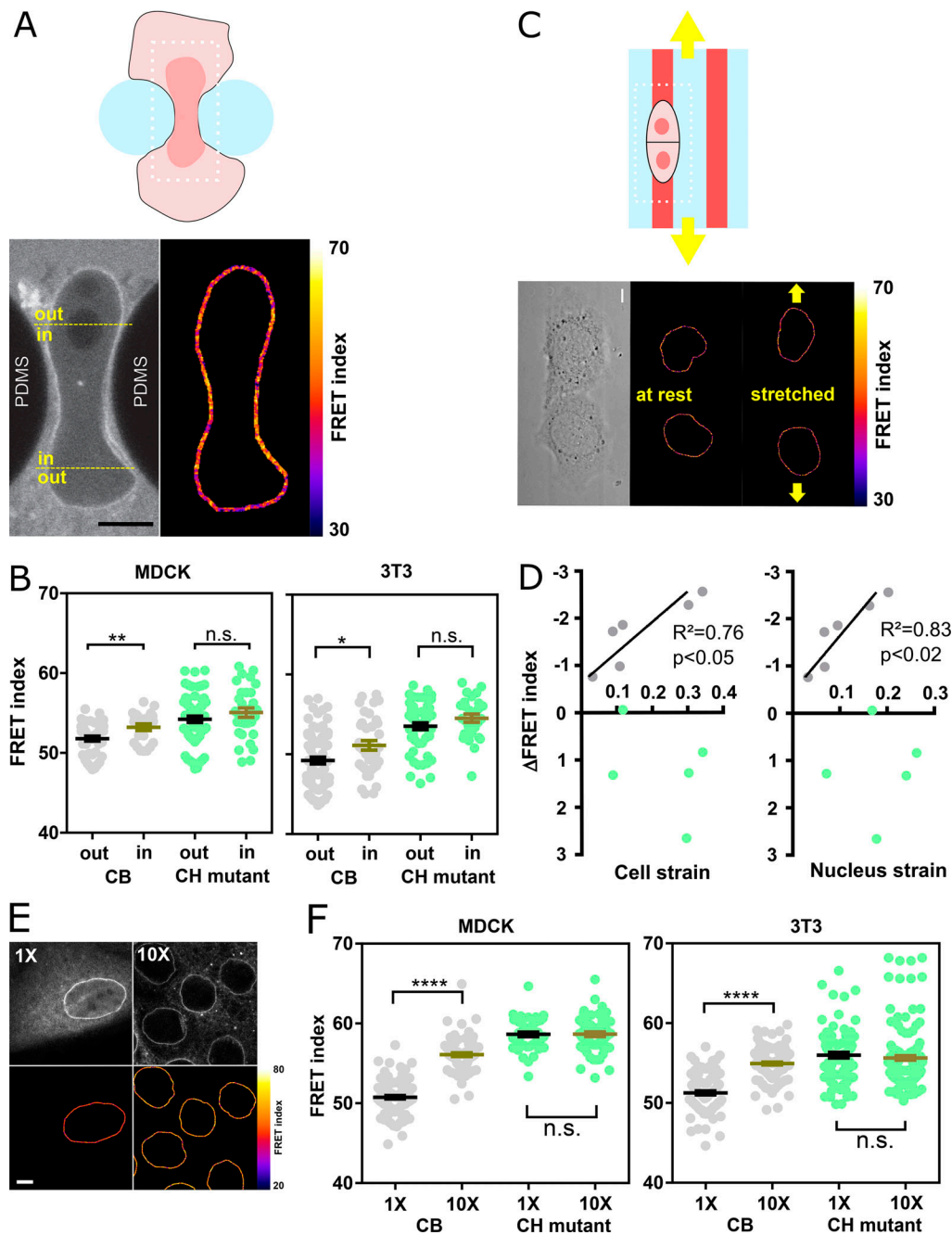
Figure 2. **Nesprin tension is sensitive to extracellular compression, stretch, and cell packing. (A)** Top: Schematics of an event of cell migration through a narrow constriction. Bottom: Direct fluorescence image and FRET index map from the dotted box above with boundaries between the region within the constriction and that outside it. **(B)** FRET index of the CB construct and the CH mutant inside and outside constrictions, in MDCK (left; n = 24 CB, 40 CH mutant) and NIH 3T3 (right; n = 48 CB out, 38 CH mutant) cells; three replicates. **(C)** Top: Schematics of the cell-stretching experiment. Cells are plated on collagen stripes printed on a transparent, elastomeric sheet stretched in the direction of the adhesive stripes. Bottom: Direct fluorescence image and FRET index map from the dotted box above. **(D)** FRET index change upon stretching of the CB construct and the CH mutant as a function cell and nucleus strains (n = 6 CB, 5 CH mutant). Solid lines are linear fits; three replicates. **(E)** MDCK cells expressing the CB construct plated at 5×10^2 cells/mm² (1×) and 5×10^3 cells/mm² (10×). Top: Fluorescence; bottom: FRET index map. **(F)** FRET index of the CB construct and the CH mutant at 1× and 10× densities in MDCK (left; n = 97 CB 1×, 82 CB 10×, 45 CH mutant 1×, 61 CH mutant 10×) and NIH 3T3 (right; n = 88 CB 1×, 120 CB 1×, 89 CH mutant 1×, 152 CH mutant 10×) cells; three replicates. Scale bar = 5 µm. Mean ± SEM. Two-tailed Mann-Whitney tests. *, P < 0.05; **, P < 0.01; ****, P < 0.0001. The color code follows that of Fig. 1.

Next, we tested whether nesprin-2G tension was sensitive to cell substrate stretching. To do so, we plated MDCK cells on adhesive patterns at the surface of a stretchable elastomer sheet substrate (Fink et al., 2011). Upon uniaxial substrate stretching, the FRET index in the CB construct significantly decreased in proportion to both cell and nucleus strains, whereas it did not in the CH mutant (Fig. 2, C and D; and Fig. S2 B). Thus, nesprin tension is sensitive to cell substrate stretching through the cytoskeleton.

Altogether, these results show that nesprin tension is sensitive through the cytoskeleton to extracellular deformations in both compression and stretch. We thus hypothesized that nesprin could sense cell packing. To test this, we compared cells plated at low density in colonies as in previous experiments (5×10^2 cells/mm²) with cells at confluence (5×10^3 cells/mm²). In cells at confluence, the nucleus cross-sectional area was much smaller (Fig. S2 C), and the CB construct exhibited a much higher FRET than in cells at low density, whereas the CH mutant did not (Fig. 2, E and F; and Fig. S2 D). Tension on nesprin is thus dependent on cell density in a manner that depends on cytoskeleton binding. Finally, our CB construct was more sensitive to cell packing (Fig. 2 F) than a construct in which the sensor module is inserted between SR2 and SR55 as previously published (Arsenovic et al., 2016; Fig. S2 E). For this reason, we used the CB construct for the rest of the study.

Nesprin tension responds to cell packing upon induction of partial EMT

Epithelial sheet wounding results in decreased cell packing at the wound edge, where cells adopt a mesenchyme-like phenotype yet migrate as a cohesive group, a model of partial EMT (Gayrard et al., 2018). Thus, we hypothesized that tension in the LINC complex would increase at the edge of a wounded sheet. In agreement, the FRET index from the CB construct exhibited in wounded MDCK and NIH 3T3 sheets a positive gradient from the wound edge back, indicative of tension at the wound edge higher than in the back of the monolayer (Fig. 3, A and B). Edge cells did not exhibit a significant difference in FRET index between the front and back of their nuclei (Fig. S3 A). Of note, the CH mutant also exhibited some FRET index decrease toward the wound edge in MDCK (but not NIH 3T3), although to a smaller extent than the CB construct, suggesting a release of some compression independent of cytoskeleton binding in this condition (Fig. 3 B and Fig. S3 B).

To assess whether increased cytoskeletal tension on nesprin is due to reduction in cell packing and not to increased cell migration velocity, we compared internuclear distance and cell velocity with FRET in cells at the edge and the bulk of a wounded monolayer, in cells at low density and confluence as above, and in cells collectively migrating within 40-μm-wide channels that maintain cell density while allowing cell migration (Fig. 3, C and D). In all these conditions, we found that FRET index correlated with internuclear distance but not with cell velocity (Fig. 3, C and D). Altogether, these results support that induction of partial EMT in a wound-healing model leads to increased tension on nesprin due to decreased cell packing rather than cell migration.

Nesprin tension does not respond to cell packing upon induction of complete EMT

Exposure of cell colonies to hepatocyte growth factor (HGF), a model of complete EMT where cells eventually migrate individually, induces decreased cell packing in the first hours before cell dissociation (Gayrard et al., 2018). Thus, we expected HGF exposure to induce an increase in tension on nesprin. To test this, we monitored how the internuclear distance, the cell spread area, and nesprin tension in MDCK colonies changed over time with or without exposure to HGF. Cells exposed to HGF exhibited a significantly larger increase in internuclear distance and cell spread area than nonexposed cells over the same time frame (Fig. 3, E–G), which confirms that HGF decreases cell packing. Unexpectedly, the FRET index of the CB but not the CH construct exhibited an increase over time, regardless of whether colonies were exposed to HGF (Fig. 3, E and H; and Fig. S3 C). These results reveal that the cytoskeletal tension exerted on nesprin has not reached a steady state in cell colonies and slowly relaxes in a time-dependent manner and density-independent manner. Indeed, the lack of difference with or without HGF shows that tension in nesprin is not responsive to cell packing upon induction of complete EMT.

Thus, nesprin exhibits distinct mechanical responses to cell packing, whether it results from induction of partial or complete EMT. The causes of this differential response may be the focus of future studies; here, we investigated its link with EMT-related signaling.

Nesprin cytoplasmic domain defines two pathways of β-catenin nuclear translocation differentially activated upon induction of partial or complete EMT

We hypothesized that the distinct mechanical responses of nesprin upon induction of partial and complete EMT would be associated with a differential regulation of β-catenin signaling. To test this, we assessed changes in the nucleoplasmic/cytoplasmic balance of α-catenin-GFP and β-catenin-GFP upon HGF stimulation of MDCK cells. HGF stimulation induced β-catenin nuclear translocation, as expected (Gayrard et al., 2018), but also that of α-catenin (Fig. 4, A and B). This is in stark contrast with the behavior of α-catenin in cells induced to undergo partial EMT in wound-healing experiments, where the release of catenins from the plasma membrane in leader cells results in nuclear translocation of β-catenin but the retention of α-catenin in the cytoplasm (Gayrard et al., 2018). Moreover, we showed that β- and α-catenin nuclear contents were reduced to levels indistinguishable from those of unstimulated cells in cells transiently expressing mCherry-DNKASH (Fig. 4, A and B), a truncated nesprin that lacks the cytoplasmic domain and displaces endogenous nesprins from the nuclear envelope (Fig. S4 A; Luxton et al., 2010). This was not the consequence of a generic impairment of nuclear translocation, because the same perturbation did not impair the translocation of the transcription factor YAP, as seen in mCherry-DNKASH cells that displayed as many YAP-positive as YAP-negative nuclei (Fig. S4 B). To assess the consequences on β-catenin–dependent transcription, we transiently expressed mCherry-DNKASH in a TOP-dGFP cell line, in which GFP expression is under the control of β-catenin transcriptional activity (Maher et al., 2009). These cells were exposed to the β-catenin degradation inhibitor LiCl for 10 h to increase β-catenin levels. In control cells, LiCl exposure resulted in GFP expression (Fig. S4 C), consistent with excess β-catenin accumulation in the nucleus (Gayrard et al., 2018). In mCherry-DNKASH–expressing cells, decreased GFP levels indicated decreased β-catenin transcriptional activity (Fig. S4 C), consistent with the loss of nuclear β-catenin upon the same perturbation (Fig. 4 A).
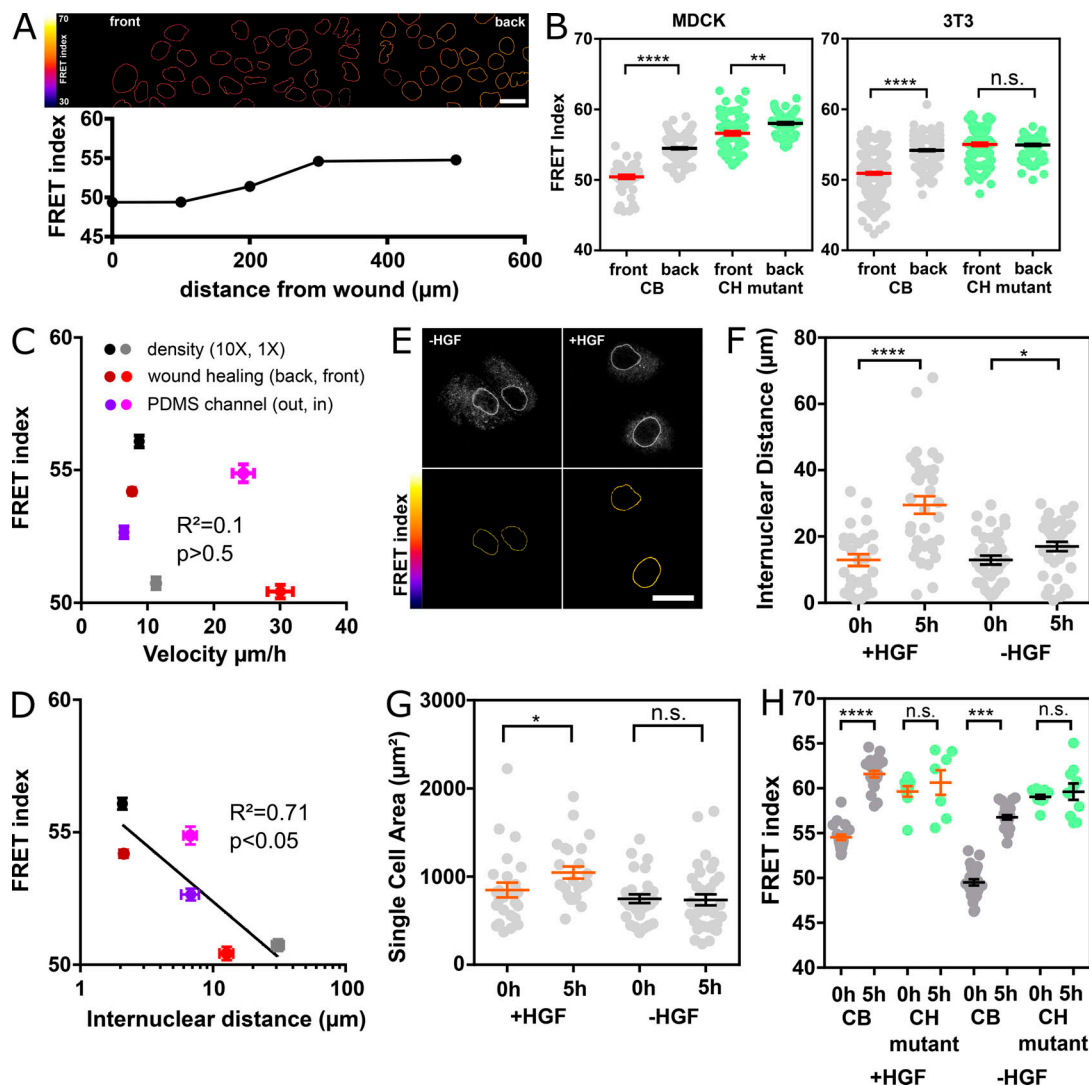
Figure 3. Nesprin tension is differentially sensitive to induction of partial and complete EMT. (A) Top: FRET index map of a wounded MDCK monolayer expressing the CB construct. Bottom: FRET index as a function of the distance from the front. **(B)** FRET index of the CB construct and the CH mutant at the front and back (500 µm) of the monolayer in MDCK (left; n = 70 CB front, 130 CB back, 73 CH mutant front, 91 CH mutant back) and NIH 3T3 (right; n = 363 CB front, 311 CB back, 125 CH mutant front, 143 CH mutant back) cells; three replicates. Solid line to guide the eye. **(C)** FRET index of the CB construct in MDCK cells as a function of cell migration velocity from experiments at low and high cell densities, upon epithelial wounding, and collectively migrating from outside (out) to inside (in) 40-µm-wide channels. R^2 was derived from a least-squares linear regression; P value was derived from an extra sum-of-squares F test with slope = 0 as the null hypothesis (n = 240 1×, 255 10×, 111 front, 110 back, 64 in, 78 out, 1 replicate). **(D)** FRET index of the CB construct in MDCK cells as a function of internuclear distance from experiments at low and high cell densities, upon epithelial wounding, and upon entering 40-µm-wide channels. Solid line is the linear fit. R^2 was derived from a least-squares linear regression; P value was derived from an extra sum-of-squares F test with slope = 0 as null hypothesis (n = 22 1×, 22 10×, 22 front, 22 back, 33 in, 18 out, 1 replicate). **(E)** Direct fluorescence and FRET index maps of the CB construct in MDCK cells after 5 h with or without HGF. **(F)** Internuclear distance of CB construct–expressing MDCK cells through time with or without HGF addition at time 0 h (n +HGF = 26 0 h, 27 5 h; n –HGF = 30 0 h, 32 5 h); two replicates. **(G)** Single-cell area of CB construct–expressing MDCK cells through time with or without HGF addition (n +HGF= 25 0 h, 24 5 h; n –HGF = 29 0 h, 35 5 h); two replicates. **(H)** FRET index of the CB construct and CH mutant in MDCK cells through time with or without HGF addition (n +HGF = 20 CB 0 h, 22 CB 5 h, 9 CH mutant 0 h, 7 CH mutant 5 h; n -HGF = 26 CB 0 h, 26 CB 5 h, 13 CH mutant 0 h, 10 CH mutant 5 h); two replicates. Scale bars = 20 µm. Mean ± SEM. Two-tailed Mann-Whitney tests. *, P < 0.05; **, P < 0.01; ***, P < 0.001; ****, P < 0.0001.

Altogether, these results support that β-catenin nuclear translocation and subsequent transcriptional activity can occur through distinct pathways: In cells induced to undergo complete EMT, nesprin is relaxed, and its cytoplasmic domain is required for β- and α-catenin nuclear translocation and β-catenin activity, whereas in cells induced to undergo partial EMT in wound-healing experiments, nesprin is tensed, and β-catenin translocates into the nucleus alone.

Nesprin relaxation recruits α-catenin to the nuclear envelope

The cytoplasmic domain of nesprin-2G contains a binding site for α-catenin in a complex with β-catenin (Neumann et al., 2010). Thus, we sought to assess whether nesprin tension could control the nuclear translocation of catenins by regulating the recruitment of α-catenin to the nuclear envelope. Consistent with this hypothesis, we found that, in HGF-stimulated cells, α-catenin accumulated at the nuclear envelope even more
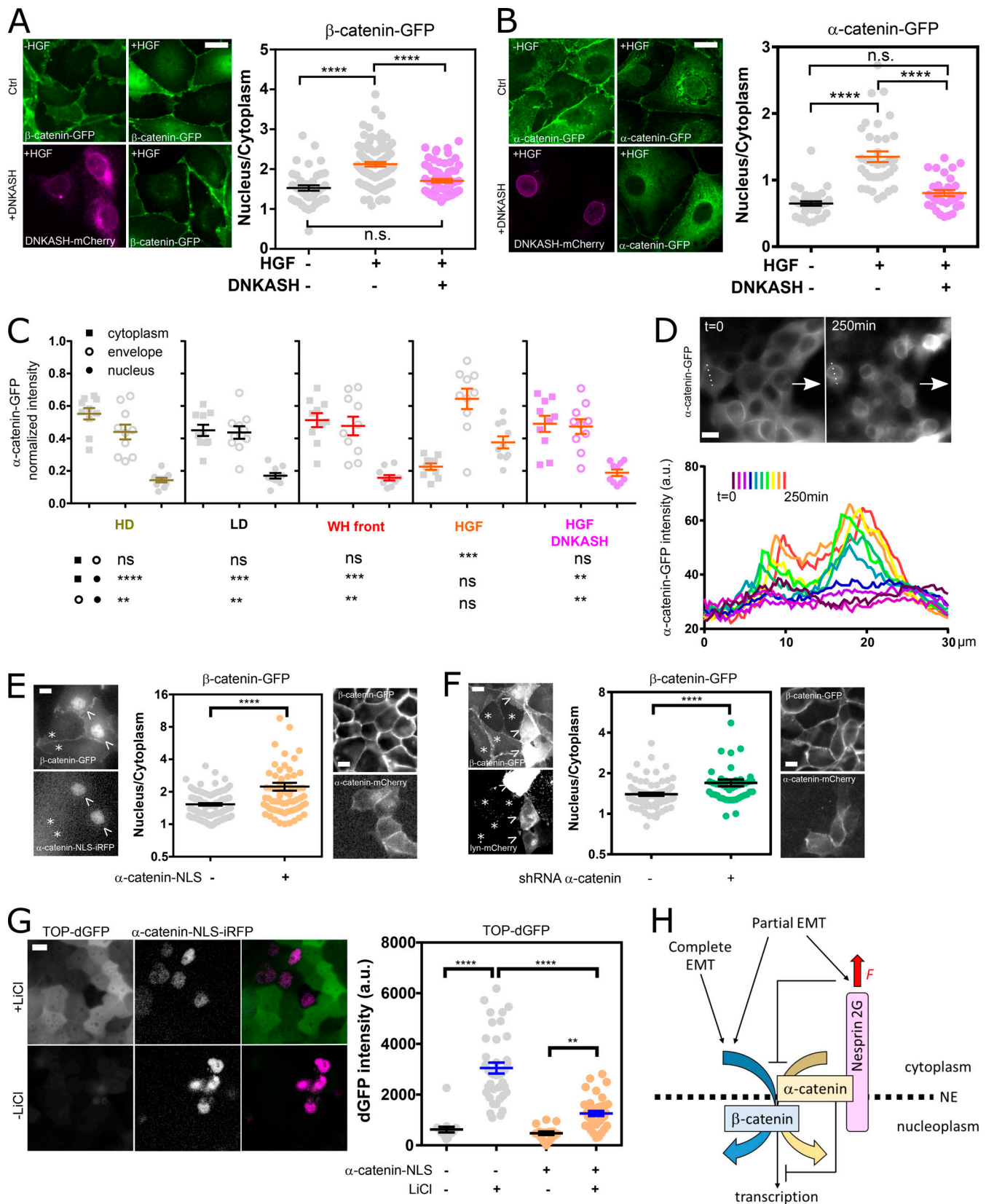
Figure 4. Nesprin tension regulates catenin nuclear translocation. (A) Left: MDCK cells stably expressing β-catenin-GFP with and without mCherry-DNKASH, with and without HGF addition. Right: β-Catenin nucleus/cytoplasmic balance (GFP intensity ratio) as a function of HGF and DNKASH (n = 43–, 89+-, 65++); one replicate. **(B)** Left: MDCK cells stably expressing α-catenin-GFP with and without mCherry-DNKASH, with and without HGF addition. Right: α-Catenin nucleus/cytoplasmic balance (GFP intensity ratio) as a function of HGF and DNKASH (n = 35–, 36+-, 31++); two replicates. **(C)** Relative cytoplasmic,

nuclear envelope, and nuclear levels of α-catenin in cells plated at high density (HD; 10×), low density (LD; 1×), at the wound front (WH, wound healing), upon HGF exposure, and upon HGF exposure and mCherry-DNKASH expression. *n* = 10 cells for each condition and compartment; two replicates. **(D)** Top: Front of collectively migrating α-catenin-GFP MDCK cells (arrows indicate direction of migration) before (t = 0) and after cytochalasin D (t = 250 min) treatment. Bottom: α-catenin-GFP intensity along dotted line above through time; one replicate. **(E)** Left: MDCK cells stably expressing β-catenin-GFP with transient expression of NLS-iRFP-α-catenin (arrowheads) and without (asterisks). Right: β-catenin nucleus/cytoplasmic balance (GFP intensity ratio) as a function of NLS-iRFP-α-catenin expression (*n* = 112-, 66+); two replicates. **(F)** Left: MDCK cells stably expressing β-catenin-GFP with transient expression of shRNA against α-catenin and lyn-mCherry (arrow) and without (asterisk). Right: β-catenin nucleus/cytoplasmic balance (GFP intensity ratio) as a function of shRNA/lyn-mCherry cotransfection (*n* = 102-, 44+); two replicates. **(G)** Left: MDCK cells stably expressing TOP-dGFP and transiently expressing NLS-iRFP-α-catenin after 10 h with and without LiCl. Right: dGFP intensity as a function of NLS-α-catenin-iRFP expression and LiCl (*n* = 17—, 39-+, 17+-, 39++); two replicates. **(H)** Working model. See text for details. Scale bars = 10 μm. Mean ± SEM. Two-tailed Kruskal-Wallis (A–C and H) and Mann-Whitney (E and F) tests. **, P < 0.01; ***, P < 0.001; ****, P < 0.0001.

than within the nucleus, and both of these accumulations were abolished in cells expressing mCherry-DNKASH, which lacks the binding site for α-catenin (Fig. 4, B and C; and Fig. S4 D). This suggests that α-catenin nuclear translocation requires its recruitment to the nuclear envelope by nesprins. Consequently, we hypothesized that increased tension on nesprin in cells induced to undergo partial EMT could explain the lack of α-catenin nuclear translocation by preventing its recruitment to the nuclear envelope. Consistently, we found no recruitment of α-catenin to the envelope compared with the cytoplasm in cells at the wound front (Fig. 4 C and Fig. S4 D). Finally, to directly test whether nesprin tension relaxation caused α-catenin recruitment to the nuclear envelope, we exposed α-catenin-GFP cells during collective migration to cytochalasin D, which relaxes nesprin (Fig. 1, D and E). Consistently, such treatment resulted in α-catenin accumulation at the nuclear envelope (Fig. 4 D). Altogether, these results show that, in cells induced to undergo complete EMT, nesprin relaxation recruits α-catenin to the nuclear envelope, whereas in cells induced to undergo partial EMT, tensed nesprin does not.

Nuclear localization of α-catenin causes β-catenin nuclear retention, but in a transcriptionally less active form

To assess the role of nuclear α-catenin in β-catenin signaling, we transiently expressed nuclear localization signal near-infrared fluorescent protein (NLS-iRFP)-α-catenin in cells stably expressing β-catenin-GFP. Compared with control cells, NLS-iRFP-α-catenin cells exhibited increased nuclear β-catenin (Fig. 4 E). In comparison, cells transiently expressing mCherry-α-catenin instead of NLS-iRFP-α-catenin did not show increased nuclear β-catenin. Thus, nuclear α-catenin promotes β-catenin nuclear localization. To determine whether α-catenin is involved in β-catenin translocation or nuclear retention, we used a shRNA that efficiently and specifically targets α-catenin (Fig. S4, E and F; Capaldo and Macara, 2007). β-catenin-GFP cells depleted by transient transfection displayed higher nuclear β-catenin levels than did nondepleted cells (Fig. 4 F). In addition, transient expression of mouse mCherry-α-catenin in depleted cells rescued low nuclear β-catenin levels (Fig. 4 F). This not only implies that α-catenin is dispensable for β-catenin nuclear translocation but also suggests that its extranuclear pool opposes constitutive β-catenin nuclear localization. Finally, we assessed the effects of nuclear α-catenin on β-catenin transcriptional activity. To do so, we transiently expressed NLS-iRFP-α-catenin in TOP-dGFP cells

exposed or not to LiCl for 10 h to increase β-catenin levels. Cells not exposed to LiCl exhibited low levels of GFP, regardless of NLS-iRFP-α-catenin expression, as expected for cells with basal β-catenin levels. In contrast, cells exposed to LiCl exhibited significantly higher GFP levels, as expected for cells with high β-catenin levels, but to a much lower extent in cells expressing NLS-iRFP-α-catenin (Fig. 4 G). Thus, nuclear α-catenin limits β-catenin transcriptional activity. Altogether, these results support that α-catenin nuclear translocation favors β-catenin nuclear localization, but in a transcriptionally less active form.

Discussion

In this work, we sought to determine whether and how the LINC complex participates in the mechanical regulation of β-catenin signaling during EMT. We found that nesprin tension increases during partial but not complete EMT. Upon induction of complete EMT, relaxation of nesprin recruits α-catenin at the nuclear envelope, which is required for the nuclear translocation of both catenins. Upon partial EMT, however, tensed nesprin does not recruit α-catenin, and β-catenin nuclear translocation occurs independently. Once in the nucleus, α-catenin sequesters β-catenin in a transcriptionally less active form.

Using an instrument-specific FRET index–to–FRET efficiency calibration (Fig. S5 A) and previously published FRET efficiency-to-force calibration (see Materials and methods), we estimate that forces exerted by the cytoskeleton on nesprin can be as high as 8 pN, the full range of the force sensor (Fig. 1). Incidentally, our results support that the nesprin cytoplasmic domain also exerts a compression force on the sensor, likely due to steric hindrance, independently of cytoskeleton binding. Such an effect can also be seen in the other SR protein α-actinin (Rahimzadeh et al., 2011) and was properly exploited to assess compression on the glycocalyx protein MUC1 (Paszek et al., 2014). As expected, smaller protein domains such as the tail of vinculin (more than four times smaller than the mini–nesprin-2G [mN2G] cytoplasmic domain) do not contribute substantially to this effect (Grashoff et al., 2010), although the protein may experience cytoskeleton binding–independent compression, too (Sarangi et al., 2017; Rothenberg et al., 2015). Nesprins thus appear to be in a constitutively compressed state that cytoskeletal tension variably releases depending on stimulations.

Remarkably, perturbation of either the actomyosin machinery or the microtubule network reduces nesprin tension. A stronger and longer colchicine treatment would likely have yielded the

opposite effect, because microtubule depolymerization results in more contractile stress fibers (Jung et al., 1997). Here, microtubule growth reduction or arrest may be just sufficient to affect nesprin tension in a fashion that may instead involve the microtubule-binding properties of CH domains (Hayashi and Ikura, 2003; Goldsmith et al., 1997), although microtubule-binding proteins typically have one CH, whereas nesprin-2G has two. Conditions aimed at mimicking cell morphological changes in a range of physiological and pathological situations all result in cytoskeleton-dependent tension changes consistent with that previously observed in cell adhesion proteins (Grashoff et al., 2010; Borghi et al., 2012).

A substantial part of cytoskeleton-dependent nesprin tension is balanced cell autonomously, as can be seen from individual cells migrating through narrow constrictions (Fig. 2). Focal adhesions, which anchor actin stress fibers to the ECM, are well positioned to play a role in this balance. Indeed, a number of adherent cells display a nesprin-dependent perinuclear actin cap with fibers terminated by focal adhesions (Khatau et al., 2009; Chambliss et al., 2013; Kim et al., 2012); cell stretching with integrin ligand-coated beads results in cytoskeleton- and nesprin-dependent nucleus stretching (Maniotis et al., 1997; Lombardi et al., 2011); and nucleus anchoring to the cytoskeleton affects cell–substrate traction forces (Shiu et al., 2018). Here, we bring a direct demonstration that nesprin tension responds to substrate mechanics: Provided that nesprin can bind to the cytoskeleton through its CH domains, its tension increases in remarkable proportion with cell and nucleus strain upon stretching of the cell substrate (Fig. 2). Although previous studies have mostly focused on isolated cells, we also show here how nesprin tension changes in a cell assembly. Remarkably, however, this tension does not necessarily correlate with that in E-cadherin, because nesprin and E-cadherin tension gradients are opposite in cells undergoing partial EMT (Fig. 3; Gayrard et al., 2018). This points to a force balance regulation that likely depends on all adhesion complexes and variable fractions of mechanically engaged proteins.

We show that cell packing is a critical determinant of nesprin tension (Fig. 2). We thus bring a direct demonstration that nesprin is a bona fide mechanosensor of cell packing at the nuclear envelope. Nevertheless, a decrease in cell packing results in an increase in nesprin tension at the front of an epithelial monolayer in partial EMT, but it does not do so upon induction of complete EMT by HGF (Fig. 3). This differential response remains unexplained, but it supports that nesprin is a mechanosensor able to discriminate between inductions of various EMT programs. This makes nesprin tension a better predictor of EMT program than E-cadherin tension or β-catenin nuclear localization. Whether this can be further harnessed in the context of diseases may be the focus of future investigations. We have previously shown that cell packing modulates β-catenin signaling downstream of focal adhesion kinase (Gayrard et al., 2018). Mechanical induction of β-catenin nuclear translocation is impaired upon disruption of the LINC complex (Uzer et al., 2018). Although nesprin-2G can interact with catenins (Neumann et al., 2010), it was unknown whether this interaction could be mechanically regulated. Here, we show that relaxation of the cytoplasmic domain of nesprin is required for α-catenin

recruitment at the nuclear envelope and catenin nuclear translocation, whereas tensed nesprin does not recruit α-catenin at the envelope, nor does it allow its nuclear translocation (Figs. 1, 3, and 4). Thus, nesprin tension controls nuclear translocation of cytoplasmic α-catenin. This supports a model whereby nesprin captures cytoplasmic catenin at the nuclear envelope for subsequent nuclear translocation in a force-dependent manner by virtue of a higher affinity in a mechanically relaxed state.

Over the last decade, a number of signaling pathways regulating proliferation have been found to respond to cell confinement and also to depend on the LINC complex, supporting a role of the latter in the former. Confinement modulates YAP/TAZ nuclear translocation and extracellular signal–regulated kinase activity cell autonomously (Dupont et al., 2011; Logue et al., 2015) and in a multicellular context (Aragona et al., 2013; Aoki et al., 2013). The nuclear translocation of YAP upon mechanical cues was shown to require the cytoplasmic domain of nesprin at the nuclear envelope (Elosegui-Artola et al., 2017). A proposed mechanism involved nesprin in transmitting cytoskeletal forces to stretch nuclear pores open and sterically facilitate nuclear translocation. Yet, YAP nuclear translocation did not always appear to require a contractile cytoskeleton (Driscoll et al., 2015). We show here that the cytoplasmic domain of nesprin, and hence tension on nesprin, is dispensable for YAP nuclear localization (Fig. S4 B). Although YAP translocation may indeed involve nuclear pore opening, our results question whether nesprin bears any mechanical function in this process, if any function at all. Finally, if nuclear pore opening were involved in β- or α-catenin translocation, it would certainly not require cytoskeletal force transmission through nesprins, because we found that β-catenin translocates regardless of nesprin tension and that α-catenin translocates upon nesprin relaxation (Figs. 1 and 4). Rather, our results support a nongeneric mechanism, such as a tension-dependent specific interaction with nesprins.

β-catenin is its own nuclear transporter that directly interacts with nuclear pore proteins (Fagotto et al., 1998), and α-catenin needs β-catenin for nuclear localization (Daugherty et al., 2014). Additionally, our results support that nuclear localization of α-catenin promotes β-catenin nuclear localization by affinity (Fig. 4). However, we show that nuclear α-catenin limits β-catenin–dependent transcription, consistent with previous reports (Giannini et al., 2000; Merdek et al., 2004; Daugherty et al., 2014; Choi et al., 2013). We thus propose that β-catenin piggybacks its own retention and transcription-limiting factor in a nesprin tension-dependent manner. In conclusion, on the basis of these results and our previous study (Gayrard et al., 2018), we propose that, in a manner dependent on the EMT program, mechanosensitive nesprins may capture, at the nuclear envelope, the catenins released from the plasma membrane when E-cadherin relaxes and thereby fine-tune their nuclear translocation and activities (Fig. 4 H).

Materials and methods

Cell lines and culture

MDCK type II G and NIH 3T3 cells were cultured at 37°C and 5% CO_2 in DMEM supplemented with 10% (vol/vol) FBS with low

glucose 1 g/liter and 100 µg/ml hygromycin for stably expressing tagged proteins of interest. Plasmids were transfected using TurboFect reagent according to the instructions of the manufacturer (Thermo Fisher Scientific). Stable cell lines were obtained by FACS after 2 wk of selection in 200 µg/ml hygromycin (InvivoGen). Cell lines expressing β-catenin-GFP, α-catenin-GFP, E-cadherin-tandem dimer RFP, and the corresponding plasmids were gifts from W.J. Nelson (Stanford University, Stanford, CA; Yamada et al., 2005; Nejsum and Nelson, 2007). The cell line expressing TOP-dGFP was a gift from C. Gottardi (Northwestern University, Chicago, IL).

Unless indicated otherwise, cells were plated on glass coverslips coated with 50 µg/ml human type IV collagen (MilliporeSigma; C7521) 24 to 48 h before imaging. Before stimulation with HGF, cells were starved for 12 h in DMEM supplemented with 0.5% FBS. Live cells were imaged in FluoroBrite DMEM (Life Technologies) without phenol red supplemented with 10% or 0.5% FBS (depending on experiments), 1 U/ml penicillin, 20 mM Hepes, and 2.5 mM L-glutamine at 37°C and 5% CO_2.

Plasmids
TSMod was obtained from the EcadTSMod construct (Borghi et al., 2012) by digestion with BspEI and SpEI. To generate the CB construct, the cytoplasmic C and transmembrane/KASH K domains of mN2G were obtained from the mN2G-GFP construct (Luxton et al., 2010) by PCR [forward (C): 5′-CTGGACTAGTGGATCCGAATTCGAGATGGCTAGCCCTGTGCTGCCC-3′; reverse (C): 5′-CTTTCGAGACTCCGGAGCCTGCTCCTGCTCCTCCACCGGTGTGGGGCATCCTGCTGTCT-3′; forward (K): 5′-GCTGTACAAGACTAGTGGTGCTGGAGGTGGTGCTGTTAACCTCGACAGCCCCGGCAGC-3′; reverse (K): 5′-TACCGAGCTCGGATCCCTAGGTGGGAGGTGGCCCGT-3′]. Digestion and PCR products were cloned into a pcDNA3.1 hygro(–) vector (Thermo Fisher Scientific) digested by BamHI using the In-Fusion HD Cloning Kit (Clontech Laboratories, TaKaRa Bio Inc.).

The CH mutant was made from the CB construct to exhibit the same mutations (I128, 131A) as previously published (Luxton et al., 2010) by site-directed mutagenesis (QuikChange II XL; Agilent Technologies; forward: 5′-CCATTATCCTTGGCCTGGCTTGGACCGCTATCCTGCACTTTCATATTG-3′; reverse: 5′-CAATATGAAAGTGCAGGATAGCGGTCCAAGCCAGGCCAAGGATAATGG-3′).

The DNKASH-TSMod construct was made by ligation after digestion by ClaI of a PCR product from the CB construct (forward: 5′-ACCATCGATGAATTCGAGATGACCGGTGGA-3′; reverse: 5′-TGCAATCGATGGATCCACTAGTCCAGTGTG-3′).

The Beyond construct was obtained by PCR on the mN2G-GFP construct (forward: 5′-GCTGTACAAGACTAGTGGTGCTGGAGGTGGTGCTGTTAACGCTAGCCCTGTGCTGCCC-3′; reverse: 5′-TACCGAGCTCGGATCCCTAGGTGGGAGGTGGCCCGT-3′). Digestion and PCR products and a synthetized double-stranded DNA linker (forward: 5′-CTGGACTAGTGGATCCGAATTCGAGATGACCGGTGGAGGAGCAGGAGCAGGCTCCGGAGTCTCGAAAG-3′) were cloned into a pcDNA3.1 hygro(–) vector as above.

The nesprin construct with TSMod between SR2 and SR55 was made as the CB construct, with primers 5′-CTTTCGAGACTCCGGAGCCTGCTCCTGCTCCTCCACCGGTGATGAAGTTTTTAC

CCAAA-3′ and 5′-GCTGTACAAGACTAGTGGTGCTGGAGGTGGTGCTGTTAACCCACTCCTGGAGCTTCAC-3′ instead of the above reverse (C) and forward (K), respectively.

The mCherry-DNKASH construct was made from the DNKASH-TSMod construct digested by AgeI/HpaI and mCherry derived from a PCR on an mCherry-cSrc construct (from M. Davidson, Florida State University, Tallahassee, FL; 55002; Addgene; forward: 5′-ATTCGAGATGACCGGTATGGTGAGCAAGGGCGAGGAGGATA-3′; reverse: 5′-GGGGCTGTCGAGGTTAACAGCACCACCTCCAGCACCCTTGTACAGCTCGTCCATGCCG-3′).

The NLS-iRFP-α-catenin construct was made from an α-catenin-GFP construct (a gift from W.J. Nelson) digested by AgeI/SalI and iRFP (Filonov et al., 2011) by PCR with the NLS sequence in the PCR primers (forward: 5′-CGCTAGCGCTACCGGTCGCCACCATGCCTGCTGCTAAAAGAGTTAAATTAGATATGGCTGAAGGATCCGTCGCCA-3′; reverse: 5′-TCATGGTGGCGTCGACTGCAGAATTCGAAGCTTGAGCTCGAGATCTGAGTCCGGACTCTTCCATCACGCCGATCTGC-3′). Constructs were verified by digestion and gel electrophoresis and sequencing of coding regions.

The shRNAs against α-catenin and lyn-mCherry plasmids were gifts from I.G. Macara (University of Virginia, Charlottesville, VA) and W.J. Nelson, respectively. The mTFP-5aa-Venus and mTFP-TRAF-Venus FRET constructs were gifts from R.N. Day (Indiana University, Bloomington, IN). The mouse mCherry-α-catenin plasmid was a gift from R.M. Mège (Institut Jacques Monod, Paris, France).

Transient genetic perturbations
Transient expression of NLS-iRFP-α-catenin and mCherry-DNKASH was obtained by transient transfection of the plasmid above using TurboFect according to the instructions of the manufacturer (Thermo Fisher Scientific). Cells were used for experiments between 48 and 72 h after transfection.

Transient depletion of α-catenin was similarly obtained with a shRNA plasmid cotransfected with a lyn-mCherry plasmid as a marker for transfected cells. In these conditions, >90% of cotransfected cells had a decrease of ~90% in α-catenin content, as shown previously (Borghi et al., 2010, 2012).

Chemical inhibitors and biochemical perturbations
HGF was used at a 50 ng/ml final concentration for 5 h on starved cells (MilliporeSigma; H5691, 20 µg/ml in PBS stock). Cytochalasin D was used at 0.5 µM final concentration for 20 min (Fig. 1) and 1 µM for 250 min (Fig. 4; MilliporeSigma; 10 mg/ml in DMSO stock). Colchicine was used at a 1 µM final concentration for 20 min (MilliporeSigma; 50 mg/ml in ethanol stock). Y27632 was used at a 10 µM final concentration for 20 min (MilliporeSigma; 10 mg/ml in water stock). EDTA was used at 1.65 µM final concentration for 20 min (Invitrogen; 0.5 M in water stock). LiCl was used at 30 mM final concentration for 10 h (105679; Merck Chemicals).

Nuclear confinement
Cells were seeded in a previously described microfluidic device, which exhibited 2-, 3-, and 5-µm-wide, 5-µm-high constrictions between adjacent 15–30-µm-wide circular polydimethylsiloxane (PDMS; Sylgard 184; Dow Corning) pillars (Davidson et al., 2015).

Stretching

As previously described (Fink et al., 2011), collagen lines (10 μm wide) were micropatterned on thin silicon membranes (Gel-Pak PF-60-X4; thickness, 150 μm). Membranes were clamped in a custom-made device allowing membrane stretching using a micrometric screw, with a maximal extension of ~25% in ~30 s. A rectangular PDMS 300-μl chamber was attached to the membrane using vacuum grease, and cells were seeded for 24 h before stretching. FRET measurements were within seconds before stretch and ~1 min afterward. Cell and nucleus strains are percentage increases in length along the stretch axis.

Wound healing and confined collective migration

For wound healing, cells were cultured at confluence around a 5 × 5–mm PDMS stencil. The PDMS stencil was removed 24 h after cell seeding and 48 h before imaging. For confined collective migration, cells were cultured at confluence around a PDMS slab exhibiting 100-μm-high, 40-μm-wide micromolded channels in contact with the coverslip. Cells were imaged 24–48 h after seeding. Cell velocities were averages of instantaneous velocities (between consecutive frames) of each cell.

FRET imaging

Spectral imaging was performed on a confocal microscope (Carl Zeiss LSM 780) with a 63×/1.4 NA Plan-Apochromat oil immersion objective. mTFP1 was excited by the 458-nm line of a 25-mW argon laser. Emission was sampled at a spectral resolution of 8.7 nm within the 476–557-nm range on a GaAsP detector. For time-lapse experiments (nuclear confinement, wound healing, and confined collective migration), images were acquired with Zen software every 10 min during ~15 h for ~10 different positions.

FRET analysis

Fluorescence images were analyzed in ImageJ software using the Fiji distribution and the publicly available PixFRET plugin. All channels were background subtracted, Gaussian smoothed (radius = 1 pixel), and thresholded (~3–5% of the 12-bit range). The FRET index E_R was computed pixel-by-pixel as $I_{EYFP}/(I_{mTFP} + I_{EYFP})$, where I_{mTFP} and I_{EYFP} are the intensities in 494-nm and 521-nm channels. Unless specified otherwise, the FRET index was then averaged over the segmented nuclear envelope for comparison between conditions. The FRET index did not display a significant dependence on the z section considered (Fig. S5 B). FRET efficiencies E were computed from FRET indices E_R with $E = (1 - a[1 - E_R]/[1 - b][1 - E_R])$, where a and b account for donor spectral bleed-through, acceptor direct excitation, and differences in donor versus acceptor absorption cross-sections and detection efficiencies (Lee et al., 2005). Measured FRET indices $E_{R,H}$ and $E_{R,L}$ (Fig. S3 A) and published FRET efficiencies E_H and E_L of mTFP-5aa-Venus and mTFP-TRAF-Venus constructs (Day et al., 2008) were used to recover $a = (E_H[1 - E_{R,H}] - E_L[1 - E_{R,L}] + E_H E_L[E_{R,H} - E_{R,L}])/c$ and $b = (E_H[1 - E_{R,L}] - E_L[1 - E_{R,H}] + E_{R,L} - E_{R,H})/c$, with $c = (E_H - E_L)(1 - E_{R,H})(1 - E_{R,L})$. Previously published FRET efficiency to force calibration (Grashoff et al., 2010) was then used to retrieve force changes, with the CH mutant used as a force-insensitive reference.

Immunostaining

Cells were fixed in 4% PFA (Electron Microscopy Sciences) for 15 min at RT, permeabilized with 0.1% or 0.5% (vol/vol) Triton X-100 in PBS for 5 min at 4°C, incubated with 50 mM NH$_4$Cl in PBS, and blocked for 30 min at RT with 1–2% BSA (Jackson ImmunoResearch or Millipore Sigma) in PBS. Cells were stained with an anti–nesprin-2 rabbit antibody directed against the CH domain of nesprin-2 (gift from G.G. Gundersen, Columbia University, New York, NY; Luxton et al., 2010; 1:500), an anti–nesprin-1 mouse antibody directed against the KASH domain of nesprin-1 (MANNES1E; gift from G.E. Morris, Wolfson Centre for Inherited Neuromuscular Disease, Oswestry, UK; Randles et al., 2010; 1:100), or an anti-YAP mouse antibody (63.7) from Santa Cruz Biotechnology (sc-101199; 1:200) in PBS with 1% BSA. Cells were then incubated with DyLight 488, DyLight 650, or Alexa Fluor 594 secondary antibodies (Thermo Fisher Scientific; 1:500). Coverslips were mounted in Fluoromount medium (MilliporeSigma) or 1:1 glycerol/PBS.

Fluorescence imaging

Non-FRET fluorescence imaging was performed either on a confocal microscope (Carl Zeiss LSM 780) with a 63×/1.4 NA oil immersion objective and Zen software, on a wide-field microscope (Carl Zeiss Axio Observer Z.1) with a 25×/0.8 NA or a 63×/1.4 NA oil immersion objective and Zen software, or on a spinning disk microscope (Roper/Nikon) with a 100×/1.4 NA oil immersion objective and MetaMorph software. On the confocal microscope, fluorophores were excited with the 488-nm line of the argon laser, the 561-nm line of the 15-mW diode-pumped solid-state laser, and the 633-nm line of the 5-mW HeNe laser, emission was collected between 498 and 561 nm, between 570 and 650 nm, and between 638 and 755 nm on photomultiplier tube detectors. On the wide-field microscope, fluorophores were excited with a light-emitting diode lamp (CoolLED pE-300 white) by using band-pass (BP) excitation filters at 450–490 nm, 500–550 nm, and 625–655 nm and dichroics at 495 nm, 555 nm, and 660 nm; and images were acquired through BP emission filters at 500–550 nm, 570–640 nm, and 665–715 nm using a scientific complementary metal–oxide–semiconductor camera (ORCA-Flash4 LT; Hamamatsu Photonics). On the spinning disk, fluorophores were excited with 491-nm and 561-nm lasers through BP excitation filters at 578–495 nm and 560–580 nm and acquired through BP emission filters at 510–555 nm and 600–650 nm on an EMCCD Evolve camera (Photometrics).

Fluorescence analysis

Fluorescence images were analyzed in ImageJ using the Fiji distribution. All channels were background subtracted. Mean pixel intensities were measured in regions of interest within the boundaries of the cytoplasm and the nucleus, as identified from nuclear envelope signals (mCherry-DNKASH or anti–nesprin-2 immunostaining) or β-catenin-GFP contrast visible with saturated intensity range when necessary. Line scan intensity was measured with a 5-pixel moving average, and anti–nesprin 2 immunostaining was used to define the nuclear envelope by colocalization and subsequently the cytoplasm and nucleus. Normalized intensities lie between the minimum (0) and

maximum (1) intensities for each condition (high density or low density).

Statistical analysis

Data are presented as mean ± SEM. P values were calculated using unpaired, nonparametric, two-tailed tests (Mann-Whitney or Kruskal-Wallis test, depending on number of conditions) in GraphPad Prism V software. R^2 values were calculated using linear regression by the least-squares method, and P values of linear regressions were calculated using an extra sum-of-squares F test with slope = 0 as the null hypothesis.

Online supplemental material

Fig. S1 shows the lack of effect of CB construct expression level on FRET, the preserved localization of nesprin-1G in cells expressing CB and CH mutant constructs, the effects of pharmacological treatments on the cytoskeleton and intercellular contacts, and the lack of effect of these treatments on the CH mutant construct. Fig. S2 shows the lack of effect of constriction, stretching, and density on the CH construct and the effect of density on nucleus section area and on a nesprin construct with the sensor inserted between SRs 2 and 55. Fig. S3 shows the lack of difference in FRET between the front and back of a nucleus within leader cells and the lack of effect of an epithelial wound or HGF treatment on the CH mutant construct. Fig. S4 shows the loss of nesprin-2G in DNKASH-positive cells, the lack of effect of DNKASH on YAP localization, the effect of DNKASH on β-catenin–dependent transcription, the localization of α-catenin in cells exposed to HGF with or without DNKASH at high and low densities and at the front of a wound, and the efficiency and specificity of the shRNA against α-catenin. Fig. S5 shows the calibration of the FRET index with FRET standards and the lack of difference of FRET in the CB construct as a function of z.

Acknowledgments

References

Aiello, N.M., R. Maddipati, R.J. Norgard, D. Balli, J. Li, S. Yuan, T. Yamazoe, T. Black, A. Sahmoud, E.E. Furth, et al. 2018. EMT subtype influences epithelial plasticity and mode of cell migration. *Dev. Cell.* 45:681–695.e4. https://doi.org/10.1016/j.devcel.2018.05.027

Alam, S.G., Q. Zhang, N. Prasad, Y. Li, S. Chamala, R. Kuchibhotla, B. KC, V. Aggarwal, S. Shrestha, A.L. Jones, et al. 2016. The mammalian LINC complex regulates genome transcriptional responses to substrate rigidity. *Sci. Rep.* 6:38063. https://doi.org/10.1038/srep38063

Aoki, K., Y. Kumagai, A. Sakurai, N. Komatsu, Y. Fujita, C. Shionyu, and M. Matsuda. 2013. Stochastic ERK activation induced by noise and cell-to-cell propagation regulates cell density-dependent proliferation. *Mol. Cell.* 52:529–540. https://doi.org/10.1016/j.molcel.2013.09.015

Aragona, M., T. Panciera, A. Manfrin, S. Giulitti, F. Michielin, N. Elvassore, S. Dupont, and S. Piccolo. 2013. A mechanical checkpoint controls multicellular growth through YAP/TAZ regulation by actin-processing factors. *Cell.* 154:1047–1059. https://doi.org/10.1016/j.cell.2013.07.042

Arsenovic, P.T., I. Ramachandran, K. Bathula, R. Zhu, J.D. Narang, N.A. Noll, C.A. Lemmon, G.G. Gundersen, and D.E. Conway. 2016. Nesprin-2G, a component of the nuclear LINC complex, is subject to myosin-dependent tension. *Biophys. J.* 110:34–43. https://doi.org/10.1016/j.bpj.2015.11.014

Borghi, N., M. Lowndes, V. Maruthamuthu, M.L. Gardel, and W.J. Nelson. 2010. Regulation of cell motile behavior by crosstalk between cadherin- and integrin-mediated adhesions. *Proc. Natl. Acad. Sci. USA.* 107: 13324–13329. https://doi.org/10.1073/pnas.1002662107

Borghi, N., M. Sorokina, O.G. Shcherbakova, W.I. Weis, B.L. Pruitt, W.J. Nelson, and A.R. Dunn. 2012. E-cadherin is under constitutive actomyosin-generated tension that is increased at cell–cell contacts upon externally applied stretch. *Proc. Natl. Acad. Sci. USA.* 109:12568–12573. https://doi.org/10.1073/pnas.1204390109

Borrego-Pinto, J., T. Jegou, D.S. Osorio, F. Auradé, M. Gorjánácz, B. Koch, I.W. Mattaj, and E.R. Gomes. 2012. Samp1 is a component of TAN lines and is required for nuclear movement. *J. Cell Sci.* 125:1099–1105. https://doi.org/10.1242/jcs.087049

Capaldo, C.T., and I.G. Macara. 2007. Depletion of E-cadherin disrupts establishment but not maintenance of cell junctions in Madin-Darby canine kidney epithelial cells. *Mol. Biol. Cell.* 18:189–200. https://doi.org/10.1091/mbc.e06-05-0471

Chambers, R., and H.B. Fell. 1931. Micro-operations on cells in tissue cultures. *Proc. R. Soc. Lond. B Biol. Sci.* 109:380–403. https://doi.org/10.1098/rspb.1931.0090

Chambliss, A.B., S.B. Khatau, N. Erdenberger, D.K. Robinson, D. Hodzic, G.D. Longmore, and D. Wirtz. 2013. The LINC-anchored actin cap connects the extracellular milieu to the nucleus for ultrafast mechanotransduction. *Sci. Rep.* 3:1087. https://doi.org/10.1038/srep01087

Chikashige, Y., C. Tsutsumi, M. Yamane, K. Okamasa, T. Haraguchi, and Y. Hiraoka. 2006. Meiotic proteins Bqt1 and Bqt2 tether telomeres to form

the bouquet arrangement of chromosomes. *Cell*. 125:59–69. https://doi.org/10.1016/j.cell.2006.01.048

Choi, S.H., C. Estarás, J.J. Moresco, J.R. Yates, III, and K.A. Jones. 2013. α-Catenin interacts with APC to regulate β-catenin proteolysis and transcriptional repression of Wnt target genes. *Genes Dev*. 27:2473–2488. https://doi.org/10.1101/gad.229062.113

Crisp, M., Q. Liu, K. Roux, J.B. Rattner, C. Shanahan, B. Burke, P.D. Stahl, and D. Hodzic. 2006. Coupling of the nucleus and cytoplasm: role of the LINC complex. *J. Cell Biol*. 172:41–53. https://doi.org/10.1083/jcb.200509124

Daugherty, R.L., L. Serebryannyy, A. Yemelyanov, A.S. Flozak, H.-J. Yu, S.T. Kosak, P. deLanerolle, and C.J. Gottardi. 2014. α-Catenin is an inhibitor of transcription. *Proc. Natl. Acad. Sci. USA*. 111:5260–5265. https://doi.org/10.1073/pnas.1308663111

Davidson, P.M., J. Sliz, P. Isermann, C. Denais, and J. Lammerding. 2015. Design of a microfluidic device to quantify dynamic intra-nuclear deformation during cell migration through confining environments. *Integr. Biol*. 7:1534–1546. https://doi.org/10.1039/C5IB00200A

Day, R.N., C.F. Booker, and A. Periasamy. 2008. Characterization of an improved donor fluorescent protein for Förster resonance energy transfer microscopy. *J. Biomed. Opt*. 13. 031203. https://doi.org/10.1117/1.2939094

Driscoll, T.P., B.D. Cosgrove, S.J. Heo, Z.E. Shurden, and R.L. Mauck. 2015. Cytoskeletal to nuclear strain transfer regulates YAP signaling in mesenchymal stem cells. *Biophys. J*. 108:2783–2793. https://doi.org/10.1016/j.bpj.2015.05.010

Dupont, S., L. Morsut, M. Aragona, E. Enzo, S. Giulitti, M. Cordenonsi, F. Zanconato, J. Le Digabel, M. Forcato, S. Bicciato, et al. 2011. Role of YAP/TAZ in mechanotransduction. *Nature*. 474:179–183. https://doi.org/10.1038/nature10137

Elosegui-Artola, A., I. Andreu, A.E.M. Beedle, A. Lezamiz, M. Uroz, A.J. Kosmalska, R. Oria, J.Z. Kechagia, P. Rico-Lastres, A.L. Le Roux, et al. 2017. Force triggers YAP nuclear entry by regulating transport across nuclear pores. *Cell*. 171:1397–1410.e14. https://doi.org/10.1016/j.cell.2017.10.008

Fagotto, F., U. Glück, and B.M. Gumbiner. 1998. Nuclear localization signal-independent and importin/karyopherin-independent nuclear import of β-catenin. *Curr. Biol*. 8:181–190. Available at: PubMed. https://doi.org/10.1016/S0960-9822(98)70082-X

Filonov, G.S., K.D. Piatkevich, L.M. Ting, J. Zhang, K. Kim, and V.V. Verkhusha. 2011. Bright and stable near-infrared fluorescent protein for in vivo imaging. *Nat. Biotechnol*. 29:757–761. https://doi.org/10.1038/nbt.1918

Fink, J., N. Carpi, T. Betz, A. Bétard, M. Chebah, A. Azioune, M. Bornens, C. Sykes, L. Fetler, D. Cuvelier, et al. 2011. External forces control mitotic spindle positioning. *Nat. Cell Biol*. 13:771–778. https://doi.org/10.1038/ncb2269

Gayrard, C., and N. Borghi. 2016. FRET-based molecular tension microscopy. *Methods*. 94:33–42. https://doi.org/10.1016/j.ymeth.2015.07.010

Gayrard, C., C. Bernaudin, T. Déjardin, C. Seiler, and N. Borghi. 2018. Src- and confinement-dependent FAK activation causes E-cadherin relaxation and β-catenin activity. *J. Cell Biol*. 217:1063–1077. https://doi.org/10.1083/jcb.201706013

Giannini, A.L., M. Vivanco, and R.M. Kypta. 2000. α-Catenin inhibits β-catenin signaling by preventing formation of a β-catenin*T-cell factor*DNA complex. *J. Biol. Chem*. 275:21883–21888. https://doi.org/10.1074/jbc.M001929200

Goldsmith, S.C., N. Pokala, W. Shen, A.A. Fedorov, P. Matsudaira, and S.C. Almo. 1997. The structure of an actin-crosslinking domain from human fimbrin. *Nat. Struct. Biol*. 4:708–712. https://doi.org/10.1038/nsb0997-708

Grady, R.M., D.A. Starr, G.L. Ackerman, J.R. Sanes, and M. Han. 2005. Syne proteins anchor muscle nuclei at the neuromuscular junction. *Proc. Natl. Acad. Sci. USA*. 102:4359–4364. https://doi.org/10.1073/pnas.0500711102

Grashoff, C., B.D. Hoffman, M.D. Brenner, R. Zhou, M. Parsons, M.T. Yang, M.A. McLean, S.G. Sligar, C.S. Chen, T. Ha, et al. 2010. Measuring mechanical tension across vinculin reveals regulation of focal adhesion dynamics. *Nature*. 466:263–266. https://doi.org/10.1038/nature09198

Guilluy, C., L.D. Osborne, L. Van Landeghem, L. Sharek, R. Superfine, R. Garcia-Mata, and K. Burridge. 2014. Isolated nuclei adapt to force and reveal a mechanotransduction pathway in the nucleus. *Nat. Cell Biol*. 16:376–381. https://doi.org/10.1038/ncb2927

Hayashi, I., and M. Ikura. 2003. Crystal structure of the amino-terminal microtubule-binding domain of end-binding protein 1 (EB1). *J. Biol. Chem*. 278:36430–36434. https://doi.org/10.1074/jbc.M305773200

Janin, A., D. Bauer, F. Ratti, G. Millat, and A. Méjat. 2017. Nuclear envelopathies: a complex LINC between nuclear envelope and pathology. *Orphanet J. Rare Dis*. 12:147. https://doi.org/10.1186/s13023-017-0698-x

Jolly, M.K., K.E. Ware, S. Gilja, J.A. Somarelli, and H. Levine. 2017. EMT and MET: necessary or permissive for metastasis? *Mol. Oncol*. 11:755–769. https://doi.org/10.1002/1878-0261.12083

Jung, H.I., I. Shin, Y.M. Park, K.W. Kang, and K.S. Ha. 1997. Colchicine activates actin polymerization by microtubule depolymerization. *Mol. Cells*. 7:431–437.

Khatau, S.B., C.M. Hale, P.J. Stewart-Hutchinson, M.S. Patel, C.L. Stewart, P.C. Searson, D. Hodzic, and D. Wirtz. 2009. A perinuclear actin cap regulates nuclear shape. *Proc. Natl. Acad. Sci. USA*. 106:19017–19022. https://doi.org/10.1073/pnas.0908686106

Kim, D.-H., S.B. Khatau, Y. Feng, S. Walcott, S.X. Sun, G.D. Longmore, and D. Wirtz. 2012. Actin cap associated focal adhesions and their distinct role in cellular mechanosensing. *Sci. Rep*. 2:555. https://doi.org/10.1038/srep00555

Lee, N.K., A.N. Kapanidis, Y. Wang, X. Michalet, J. Mukhopadhyay, R.H. Ebright, and S. Weiss. 2005. Accurate FRET measurements within single diffusing biomolecules using alternating-laser excitation. *Biophys. J*. 88:2939–2953. https://doi.org/10.1529/biophysj.104.054114

Logue, J.S., A.X. Cartagena-Rivera, M.A. Baird, M.W. Davidson, R.S. Chadwick, and C.M. Waterman. 2015. Erk regulation of actin capping and bundling by Eps8 promotes cortex tension and leader bleb-based migration. *eLife*. 4. e08314. https://doi.org/10.7554/eLife.08314

Lombardi, M.L., D.E. Jaalouk, C.M. Shanahan, B. Burke, K.J. Roux, and J. Lammerding. 2011. The interaction between nesprins and SUN proteins at the nuclear envelope is critical for force transmission between the nucleus and cytoskeleton. *J. Biol. Chem*. 286:26743–26753. https://doi.org/10.1074/jbc.M111.233700

Luxton, G.W.G., E.R. Gomes, E.S. Folker, E. Vintinner, and G.G. Gundersen. 2010. Linear arrays of nuclear envelope proteins harness retrograde actin flow for nuclear movement. *Science*. 329:956–959. https://doi.org/10.1126/science.1189072

Maher, M.T., A.S. Flozak, A.M. Stocker, A. Chenn, and C.J. Gottardi. 2009. Activity of the β-catenin phosphodestruction complex at cell–cell contacts is enhanced by cadherin-based adhesion. *J. Cell Biol*. 186:219–228. https://doi.org/10.1083/jcb.200811108

Maniotis, A.J., C.S. Chen, and D.E. Ingber. 1997. Demonstration of mechanical connections between integrins, cytoskeletal filaments, and nucleoplasm that stabilize nuclear structure. *Proc. Natl. Acad. Sci. USA*. 94:849–854.

Merdek, K.D., N.T. Nguyen, and D. Toksoz. 2004. Distinct activities of the α-catenin family, α-catulin and α-catenin, on β-catenin-mediated signaling. *Mol. Cell. Biol*. 24:2410–2422. Available at: http://www.ncbi.nlm.nih.gov/pubmed/14993280.

Nejsum, L.N., and W.J. Nelson. 2007. A molecular mechanism directly linking E-cadherin adhesion to initiation of epithelial cell surface polarity. *J. Cell Biol*. 178:323–335. https://doi.org/10.1083/jcb.200705094

Neumann, S., M. Schneider, R.L. Daugherty, C.J. Gottardi, S.A. Eming, A. Beijer, A.A. Noegel, and I. Karakesisoglou. 2010. Nesprin-2 interacts with α-catenin and regulates Wnt signaling at the nuclear envelope. *J. Biol. Chem*. 285:34932–34938. https://doi.org/10.1074/jbc.M110.119651

Paszek, M.J., C.C. DuFort, O. Rossier, R. Bainer, J.K. Mouw, K. Godula, J.E. Hudak, J.N. Lakins, A.C. Wijekoon, L. Cassereau, et al. 2014. The cancer glycocalyx mechanically primes integrin-mediated growth and survival. *Nature*. 511:319–325. https://doi.org/10.1038/nature13535

Rahimzadeh, J., F. Meng, F. Sachs, J. Wang, D. Verma, and S.Z. Hua. 2011. Real-time observation of flow-induced cytoskeletal stress in living cells. *Am. J. Physiol. Cell Physiol*. 301:C646–C652. https://doi.org/10.1152/ajpcell.00099.2011

Randles, K.N., T. Lam, C.A. Sewry, M. Puckelwartz, D. Furling, M. Wehnert, E.M. McNally, and G.E. Morris. 2010. Nesprins, but not SUN proteins, switch isoforms at the nuclear envelope during muscle development. *Dev. Dyn*. 239:998–1009. https://doi.org/10.1002/dvdy.22229

Rothenberg, K.E., S.S. Neibart, A.S. LaCroix, and B.D. Hoffman. 2015. Controlling cell geometry affects the spatial distribution of load across vinculin. *Cell. Mol. Bioeng*. 8:364–382. https://doi.org/10.1007/s12195-015-0404-9

Sarangi, B.R., M. Gupta, B.L. Doss, N. Tissot, F. Lam, R.-M. Mège, N. Borghi, and B. Ladoux. 2017. Coordination between intra- and extracellular forces regulates focal adhesion dynamics. *Nano Lett*. 17:399–406. https://doi.org/10.1021/acs.nanolett.6b04364

Shiu, J.-Y., L. Aires, Z. Lin, and V. Vogel. 2018. Nanopillar force measurements reveal actin-cap-mediated YAP mechanotransduction. *Nat. Cell Biol*. 20:262–271. https://doi.org/10.1038/s41556-017-0030-y

Starr, D.A., and M. Han. 2002. Role of ANC-1 in tethering nuclei to the actin cytoskeleton. *Science*. 298:406–409. https://doi.org/10.1126/science.1075119

Swartz, R.K., E.C. Rodriguez, and M.C. King. 2014. A role for nuclear envelope–bridging complexes in homology-directed repair. *Mol. Biol. Cell.* 25:2461–2471. https://doi.org/. https://doi.org/10.1091/mbc.e13-10-0569

Tajik, A., Y. Zhang, F. Wei, J. Sun, Q. Jia, W. Zhou, R. Singh, N. Khanna, A.S. Belmont, and N. Wang. 2016. Transcription upregulation via force-induced direct stretching of chromatin. *Nat. Mater.* 15:1287–1296. https://doi.org/10.1038/nmat4729

Uzer, G., G. Bas, B. Sen, Z. Xie, S. Birks, M. Olcum, C. McGrath, M. Styner, and J. Rubin. 2018. SUN-mediated mechanical LINC between nucleus and cytoskeleton regulates βcatenin nuclear access. *J. Biomech.* 74:32–40. https://doi.org/10.1016/j.jbiomech.2018.04.013

Wang, S., E. Stoops, U. Cp, B. Markus, A. Reuveny, E. Ordan, and T. Volk. 2018. Mechanotransduction via the LINC complex regulates DNA replication in myonuclei. *J. Cell Biol.* 217:2005–2018. https://doi.org/10.1083/jcb.201708137

Yamada, S., S. Pokutta, F. Drees, W.I. Weis, and W.J. Nelson. 2005. Deconstructing the cadherin–catenin–actin complex. *Cell.* 123:889–901. Available at: http://www.sciencedirect.com/science/article/B6WSN-4HPCH8Y-R/2/769e6e6d57d3009d22d68c30eefec435.
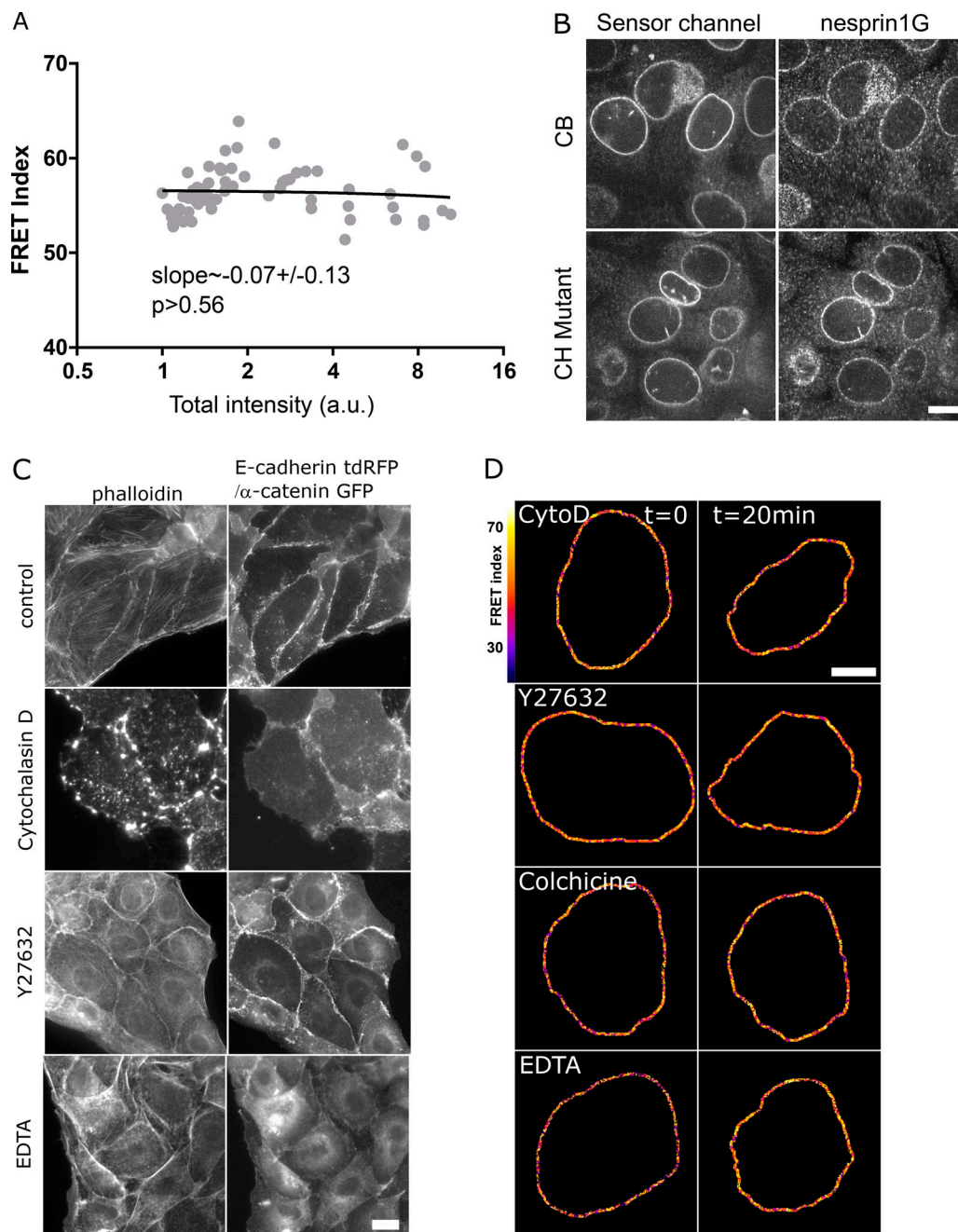
Supplemental material

Figure S1. **Validation of CB and CH mutant constructs, with drug treatments. (A)** FRET index of the CB construct as a function of its transient expression level in MDCK cells (n = 64; total intensity is the emission intensity sum between 476 and 557 nm encompassing both donor and acceptor emissions); one replicate. Solid line is a linear fit (least-squares linear regression); P value was derived from an extra sum-of-squares F test with slope = 0 as null hypothesis. **(B)** Nuclear envelope localization of nesprin-1G by immunofluorescence in cells expressing either the CB or the CH mutant construct. Scale bar = 10 μm. **(C)** Effects of pharmacological treatments on the cytoskeleton. E-cadherin-tandem dimer RFP (two first rows) or α-catenin-GFP cells (other rows, to visualize intercellular contacts) treated as in Fig. 1 D. Control cells exhibit F-actin at contacts and at the ventral surface. Cytochalasin D resulted in dense actin aggregates, Y27632 in an altered cytoplasmic organization with some nuclear envelope recruitment at the expense of ventral stress fibers, and EDTA in a loss of intercellular contacts and subsequent recruitment. Scale bar = 10 μm. **(D)** FRET index map of the CH construct in MDCK cells before and after pharmacological perturbations. Cyto D, cytochalasin D. Compare with Fig. 1 D. Scale bar = 5 μm.
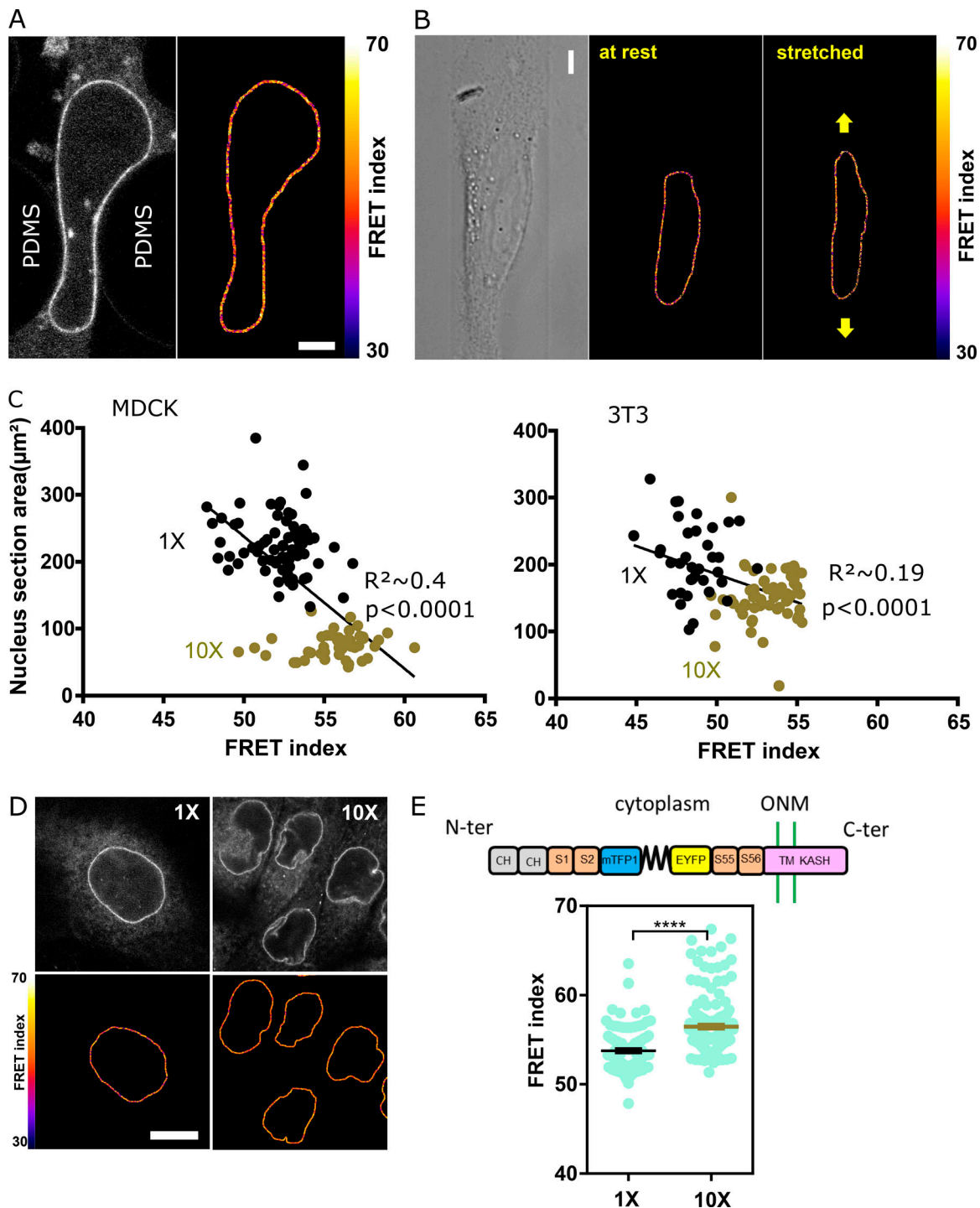
Figure S2. **Effects of mechanical perturbations on the CH mutant and nesprin with sensor between SR2 and 55 constructs. (A)** Direct fluorescence image and FRET index map of an MDCK cell expressing the CH construct within a constriction. Compare with Fig. 2 A. Scale bar = 5 μm. **(B)** Direct fluorescence image and FRET index map of an MDCK cell expressing the CH construct plated on a collagen stripe on the stretchable substrate. Compare with Fig. 2 C. Scale bar = 5 μm. **(C)** Nucleus section area as a function of FRET index for low (1×) and high (10×) cell densities for MDCK (top; n = 73 1×, 45 10×) and NIH 3T3 (right; n = 36 1×, 59 10×) cells; two replicates. Solid lines are linear fits (R^2 was derived from a least-squares linear regression; P value was derived from an extra sum-of-squares F test with slope = 0 as null hypothesis). **(D)** MDCK cells expressing the CH construct plated at 5 × 10^2 cells/mm^2 (1×) and 5 × 10^3 cells/mm^2 (10×). Top: Fluorescence, bottom: FRET index map. Compare with Fig. 2 E. Scale bar = 10 μm. **(E)** Top: Schematic illustration of the nesprin construct with the tension sensor inserted between spectrin repeats 2 and 55. ONM, outer nuclear membrane; S1...S56, spectrin repeat number; TM, trans-membrane domain. Bottom: FRET index of the construct illustrated above at 1× and 10× densities in MDCK cells (n = 93 1×, 184 10×). Compare with Fig. 2 F. Mean ± SEM. Two-tailed Mann-Whitney test. ****, P < 0.0001.
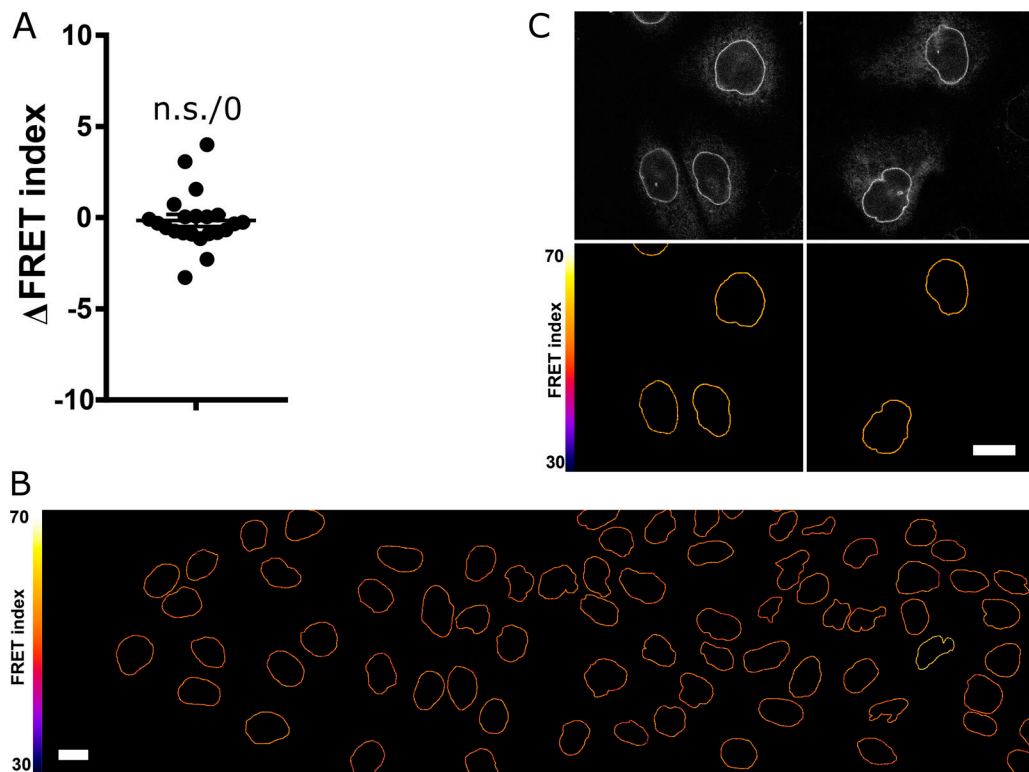
Figure S3. **Effects of nuclear localization of the CB construct on its tension and of wounding and HGF on the CH mutant construct. (A)** FRET index difference between the front and back of a nucleus within leader cells (n = 22); one replicate. Mean ± SEM. Two-tailed Kruskal-Wallis test. **(B)** FRET index map of a wounded MDCK monolayer expressing the CH construct. Compare with Fig. 3 A. Scale bar = 10 µm. **(C)** Direct fluorescence and FRET index maps of the CH construct in MDCK cells after 5 h with or without HGF. Compare with Fig. 3 E. Scale bar = 10 µm.
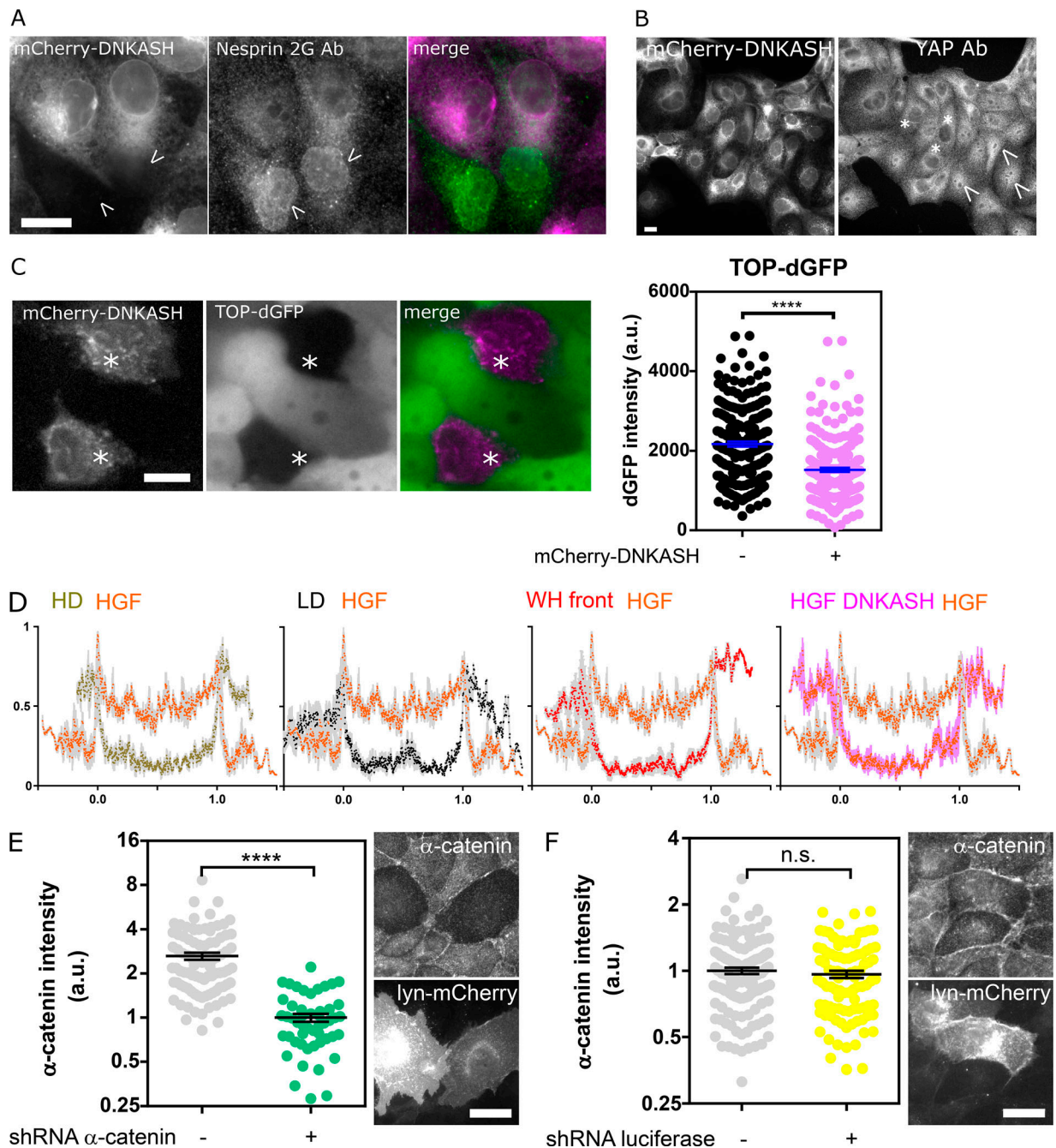
Figure S4. **Validation and specificity of the DNKASH construct and α-catenin depletion. (A)** MDCK cells transiently expressing mCherry-DNKASH and stained for nesprin 2G. Only nontransfected cells (arrowheads) show nesprin 2G localization at the nuclear envelope. **(B)** MDCK cells stably expressing mCherry-DNKASH and stained for YAP. Some cells display nuclear YAP (arrowheads), and some do not (asterisks). **(C)** MDCK cells stably expressing TOP-dGFP and transiently expressing mCherry-DNKASH after 10 h with LiCl. Cells expressing mCherry-DNKASH (asterisks) show lower dGFP levels (n = 216 +mCherry-DNKASH, 216 -mCherry-DNKASH); two replicates. **(D)** Normalized α-catenin-GFP intensity along a line scan across the nucleus of cells exposed to HGF compared with that of cells plated at high (HD; 10×) and low (LD; 1×) densities, at the front of an epithelial wound, and expressing mCherry-DNKASH with HGF; two replicates. Line scans are averages of three cells, 5 pixels window moving average. 0 and 1 are nuclear envelope positions. **(E)** Immunofluorescence intensity of α-catenin in MDCK cells cotransfected with a lyn-mCherry construct (as a marker of transfection) and a shRNA against α-catenin (n = 50 sh-, 89 sh+); one replicate. **(F)** Immunofluorescence intensity of α-catenin in MDCK cells cotransfected with a lyn-mCherry construct and a shRNA against luciferase (n = 97 sh-, 131 sh+); one replicate. Scale bars = 10 μm. Mean ± SEM. Two-tailed Mann-Whitney test (F); Kruskal-Wallis test otherwise. ****, P < 0.0001.
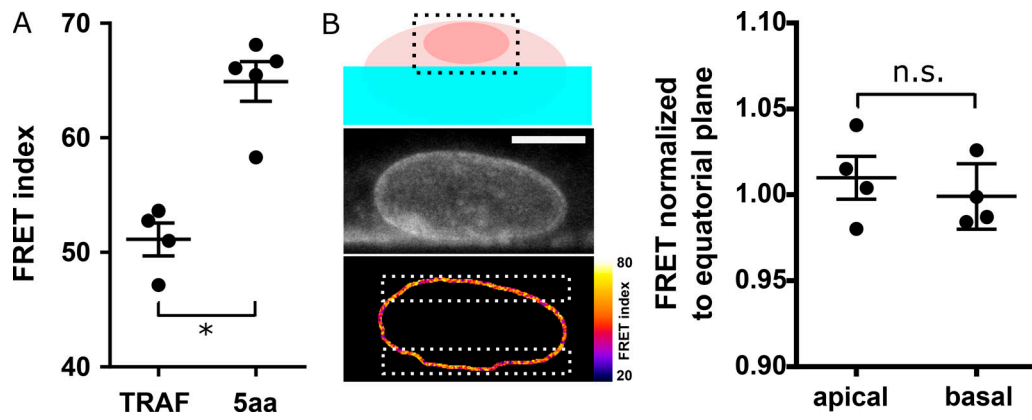
Figure S5.   **FRET calibration and tension dependence on z. (A)** FRET index of 5aa and TRAF standards expressed in MDCK cells ($n = 4$); one replicate. **(B)** Left: Sketch of a cell growing on the side of a PDMS channel for FRET analysis along z. Direct fluorescence and FRET index of an MDCK cell stably expressing the CB construct from the region in the dotted box above. Right: Normalized FRET index from the white dotted boxes on the left ($n = 4$); one replicate. Scale bar = 5 µm. Mean ± SEM. Two-tailed Kruskal-Wallis test. *, $P < 0.05$.